# Down-regulation of the islet-specific zinc transporter-8 (ZnT8) protects human insulinoma cells against inflammatory stress

Received for publication, September 5, 2019, and in revised form, October 4, 2019 Published, Papers in Press, October 7, 2019, DOI 10.1074/jbc.RA119.010937

**Chengfeng Merriman and Dax Fu**[1]

*From the Department of Physiology, Johns Hopkins School of Medicine, Baltimore, Maryland 21205*

Edited by Jeffrey E. Pessin

**Zinc transporter-8 (ZnT8) primarily functions as a zinc-sequestrating transporter in the insulin-secretory granules (ISGs) of pancreatic β-cells. Loss-of-function mutations in ZnT8 are associated with protection against type-2 diabetes (T2D), but the protective mechanism is unclear. Here, we developed an in-cell ZnT8 assay to track endogenous ZnT8 responses to metabolic and inflammatory stresses applied to human insulinoma EndoC-βH1 cells. Unexpectedly, high glucose and free fatty acids did not alter cellular ZnT8 levels, but proinflammatory cytokines acutely, reversibly, and gradually down-regulated ZnT8. Approximately 50% of the cellular ZnT8 was localized to the endoplasmic reticulum (ER), which was the primary target of the cytokine-mediated ZnT8 down-regulation. Transcriptome profiling of cytokine-exposed β-cells revealed an adaptive unfolded protein response (UPR) including a marked immunoproteasome activation that coordinately degraded ZnT8 and insulin over a 1,000-fold cytokine concentration range. RNAi-mediated *ZnT8* knockdown protected cells against cytokine cytotoxicity, whereas inhibiting immunoproteasomes blocked cytokine-induced ZnT8 degradation and triggered a transition of the adaptive UPR to cell apoptosis. Hence, cytokine-induced down-regulation of the ER ZnT8 level promotes adaptive UPR, acting as a protective mechanism that decongests the ER burden of ZnT8 to protect β-cells from proapoptotic UPR during chronic low-grade inflammation.**

Pancreatic β-cells dedicate up to 50% of biosynthetic capacity to insulin production upon glucose stimulation (1). The synthesized insulins are complexed with zinc to form solid zinc-insulin crystals for storage in ISGs,[2] giving rise to one of the highest quantities of cellular zinc in the human body (2, 3). The granular zinc is secreted along with insulin and then recycled back into β-cells during iterative cycles of insulin secretion and restocking. This dynamic process demands tight controls over zinc transport to achieve coordinated zinc mobilization while maintaining the cytosolic free zinc concentration around a homoeostatic setpoint (4). Among all of the zinc transporters in β-cells (5, 6), ZnT8 is unique in its islet-specific expression (7, 8), and its high abundance as a major autoantigen involved in autoimmunity of type-1 diabetes (T1D) (9, 10). Human genetics revealed that a hyperactive ZnT8 polymorphic variant encoded by the *SLC30A8* gene was associated with increased T2D risk (11), whereas nonsense/frameshift mutations in *SLC30A8* were found to be protective against T2D in heterozygous human carriers (12). The emerging evidence supports a causality linking ZnT8 down-regulation to reduced T2D risk, but the protective mechanism of ZnT8 down-regulation is unclear.

The onset of T2D and its progression are largely determined by a progressive failure of β-cells to produce sufficient amounts of insulin to compensate for insulin resistance. Multiple ZnT8 null mouse models showed a consistent decrease of ISG zinc content (13–17) but variable phenotypic changes in glucose-stimulated insulin secretion (GSIS) (18). Apparently, the transport activity of ZnT8 is not closely associated with GSIS, raising the possibility that novel aspects of ZnT8 cell biology may regulate β-cell resilience to stress-induced failure. A major stress factor for T2D is the deleterious consequences of overnutrition (19). Chronic exposures to high levels of glucose and FFA impair insulin secretion, induce β-cell death, and promote insulin resistance (20, 21). A combination of elevated glucose and FFA has a potentiating effect known as glucolipotoxicity (22). Excessive levels of glucose and FFA can also induce local production and release of cytokines and chemokines from pancreatic islets, leading to macrophage recruitment and islet inflammation characterized by increased expression of inflammatory cytokines derived from innate immune cells (23). This local inflammation is exacerbated by circulating cytokines released from nutrient-stressed adipose tissues (24–26). Moreover, β-cells under metabolic and inflammatory stresses overproduce hydroxyl radicals (*OH) and nitroxide (NO) by mitochondrial oxidation and inducible nitric-oxide synthase, respectively (27, 28). Zinc is an essential co-factor for enzymes

This work was supported by NIGMS, National Institutes of Health, Grant R01 GM065137. The authors declare that they have no conflicts of interest with the contents of this article. The content is solely the responsibility of the authors and does not necessarily represent the official views of the National Institutes of Health.

*The RNA-Seq data are available from the National Center for Biotechnology Information Gene Expression Omnibus (GEO) under accession number GSE134122.*

[1] To whom correspondence should be addressed: Dept. of Physiology, Johns Hopkins School of Medicine, 725 N. Wolfe St., Baltimore, MD 21205. Tel.: 443-287-4941; E-mail: dfu3@jhmi.edu.

[2] The abbreviations used are: ISG, insulin-secretory granule; T1D, type-1 diabetes; T2D, type-2 diabetes; GSIS, glucose-stimulated insulin secretion; FFA, free fatty acid(s); ER, endoplasmic reticulum; HRP, horseradish peroxidase; LOQ, limit of quantification; PA, palmitic acid; IL, interleukin; IFN, interferon; TNF, tumor necrosis factor; MSC, Manders' split coefficient; ROI, region of interest; pAb, polyclonal antibody; SCD, stearoyl-CoA desaturase; FPKM, fragments per kilobase of transcript per million; ERAD, ER-associated protein degradation; NHS, *N*-hydroxylsuccinimide; SUV, small unilamellar vesicle; UPR, unfolded protein response.

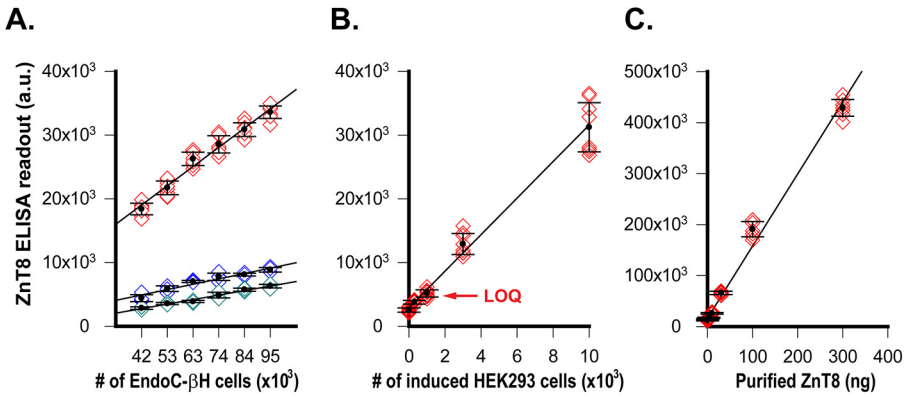


**Figure 1. Assay calibration.** *A*, linear response of ZnT8-ELISA readout with an increasing number of EndoC-βH1 (*red*), INS-1E (*blue*), and HEK293 cells (*dark cyan*). *Solid lines*, linear regressions of mean values of 4–8 replicated measurements for each data point. *Error bars*, S.D. The coefficient of determination ($r^2$) for fitted regression lines ranges from 0.98 to 1.00. *B*, linear response of ZnT8-ELISA readout with increasing ZnT8 expression in HEK293 cells ($r^2 = 1.00$). The number of ZnT8-expressing cells in each well was increased from 0 to $10 \times 10^3$, and the number of ZnT8-negative cells was adjusted to give a total number of $30 \times 10^3$ cells in each well. ZnT8 expression was induced by doxycycline for 16 h. LOQ is 10× S.D. above the background. *C*, linear response of ZnT8-ELISA readout to purified ZnT8.

involved in the proper functioning of the antioxidant defense system (29). Perturbation of zinc homeostasis could intensify oxidative stress and cell damage (30). At the cellular level, metabolic, inflammatory, and zinc stress converge to activate UPR that could either allow cells to survive by adapting to stress or kill cells through apoptosis (31). Characterizing stress-induced ZnT8 responses in adaptive UPR may illuminate how ZnT8 influences the UPR decision on β-cell fate, thereby providing information on the protective mechanism of ZnT8 down-regulation.

A major challenge to track adaptive UPR is the lack of a detectable change in cell viability. In the present study, we used stress-induced fluctuations of the endogenous ZnT8 level as a phenotypic readout. Toward this end, we generated an anti-ZnT8 mAb (mAb20) with superb specificity for in-cell ZnT8 immunodetection over a low background of nonspecific bindings to other ZnT paralogs and high-abundance cellular proteins in EndoC-βH1 cells (32). Built on mAb20, an in-cell ELISA was developed to quantify fluctuations of the endogenous ZnT8 level in a multifactorial space of glucose (Glc), FFA, zinc, proinflammatory cytokines, and their time- and dose-dependent profiles. This precise assay revealed a highly sensitive ZnT8 response to cytokine stimulations. Further analysis revealed a pleiotropic role of ZnT8 in the ER, where ZnT8 and insulin were selectively targeted as two major β-cell autoantigens for immunoproteasome-mediated degradation. Hence, our experiments revealed a novel immunologic process of decongesting two major ER burdens to protect β-cells from proapoptotic UPR.

## Results

### *Assay validation*

A ZnT8-specific ELISA was developed to track the endogenous ZnT8 level in EndoC-βH1 cells immobilized to a 96-well plate by paraformaldehyde fixation, followed by immunostaining and horseradish peroxidase (HRP) chemiluminescence. The nonspecific background was estimated using rat insulinoma INS-1E and human HEK293 cells as negative controls. We tested two recently developed anti-ZnT8 mAbs (mAb20 and mAb39). Although both mAbs had a subnanomolar binding affinity (33), only mAb20 had a significant signal-to-noise ratio when endogenous ZnT8 in EndoC-βH1 cells was probed at a saturating mAb concentration (1:600 dilution). Assay calibration showed a linear increase in the HRP readout with a cell number that was proportional to the amount of endogenous ZnT8 (Fig. 1*A*). The signal-to-noise ratio at $95 \times 10^3$ cells was 3.9 (Z′ score = 0.8) over a background detected from the same number of INS-1E cells (Fig. 1*A*). The nonspecific background was further reduced for HEK293 cells with negative ZnT8 expression (Fig. 1*A*). Mixing HEK293 cells with and without heterologous ZnT8 expression showed a linear ZnT8-ELISA response extending to a limit of quantification (LOQ) (Fig. 1*B*) corresponding to ~1,000 HEK293 cells with doxycycline-induced ZnT8 expression under a Tet repressor (34). Assay calibration using purified human ZnT8 immobilized to a nickel-nitrilotriacetic acid plate via a C-terminal His tag also yielded a linear ELISA response (Fig. 1*C*).

### *ZnT8 responses to metabolic and zinc stress*

We used ZnT8-ELISA to characterize endogenous ZnT8 responses to T2D-relevant stimuli. It was well-established that elevated Glc/FFA levels acutely increased β-cell mass and insulin production, but continuous exposures led to glucolipotoxicity (35). Accordingly, we used a mixture of Glc and palmitic acid (PA) to mimic metabolic stress and measured the dose response of endogenous ZnT8 to serial dilutions of the mixture starting from 48 mM Glc plus 0.6 mM PA. At a fixed time point of 24 h after metabolic stress, the endogenous ZnT8 level in EndoC-βH1 cells showed small fluctuations within experimental errors (Fig. 2*A*). By comparison, the endogenous ZnT8 level showed a biphasic change when the extracellular zinc concentration was progressively increased from a trace amount by EDTA chelation to 600 μM (Fig. 2*B*). The biphasic profile peaked around 10 μM zinc, indicating that the cellular ZnT8 level was first up- and then down-regulated in response to a switch of the zinc status from deficiency to overload.

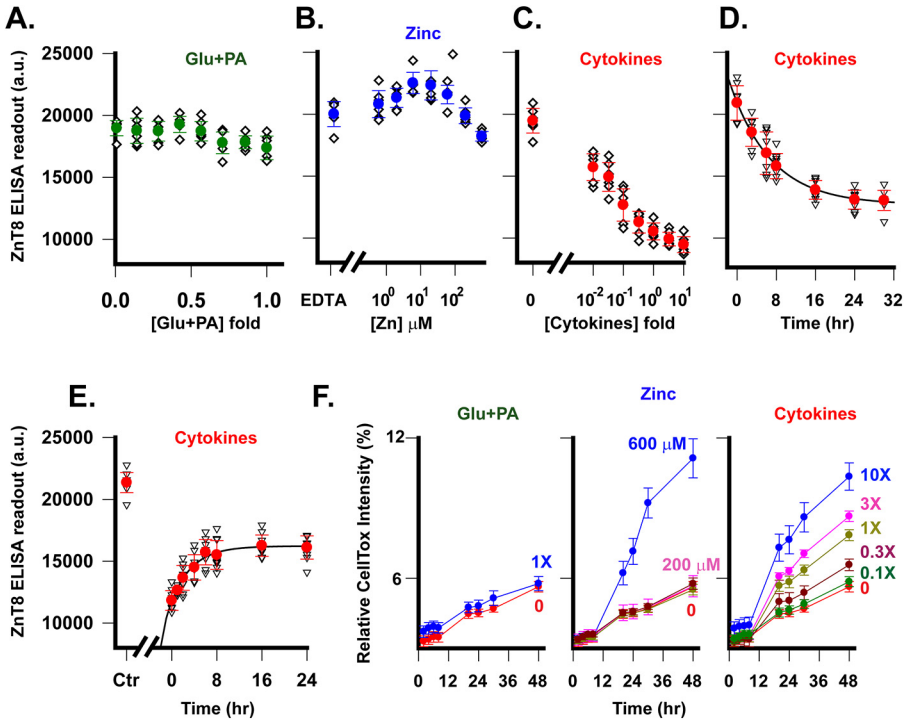


**Figure 2. Perturbation of endogenous ZnT8 expression.** *A–C*, dose responses of the endogenous ZnT8 level as a function of Glc + PA (*green*), zinc (*blue*) or cytokine concentration (*red*). *Filled circles*, means of eight replicated measurements (*diamonds*) with S.D. values shown as *error bars*. *D*, time course of cytokine-induced ZnT8 down-regulation. *Solid line*, an exponential fit of the time course ($r^2 = 0.99$). *Error bars*, S.D. of eight replicated measurements from one representative experiment. *E*, time course of ZnT8 recovery after removal of cytokines at $t = 0$. *Ctr*, untreated control. *Solid line*, exponential fit of the time course ($r^2 = 0.99$). *F*, time courses of normalized CellTox fluorescence intensities in response to different concentrations of Glc + PA, zinc, and cytokine exposures as indicated. The relative CellTox fluorescence intensity was normalized to that induced by detergent-induced cell lysis. *Filled circles*, means of eight replicated measurements; *error bars*, S.D. *a.u.*, arbitrary units.

### *ZnT8 response to inflammatory stress*

The pancreatic $\beta$-cell is a target of cytokines as inflammatory mediators of functional suppression and cell death during the development of both T1D and T2D (25, 36). We used a master cytokine mixture consisting of IL-1$\beta$ (5 ng/ml), IFN-$\gamma$ (50 ng/ml), IL-17 (100 ng/ml) and TNF$\alpha$ (10 ng/ml) to mimic the *in vivo* cytokine load in islet inflammation (37). EndoC-$\beta$H1 cells were exposed to a sequence of cytokine concentrations ranging from 0.01- to 10-fold the master concentration. After a 24-h cytokine exposure, the endogenous ZnT8 level showed a graded reduction with increasing cytokine concentrations, reaching a steady state at 48.6% of the untreated control (Fig. 2*C*). Next, we examined the time course of cytokine actions. At a fixed 1× cytokine concentration, cytokine exposure induced an exponential decay of the endogenous ZnT8 level with a time constant of 8.5 ± 0.3 h (Fig. 2*D*). Next, we examined the reversibility of cytokine-induced ZnT8 down-regulation. EndoC-$\beta$H1 cells were first exposed to a 1× cytokine mixture for 24 h and then recovered in a cytokine-free medium for different time periods. The endogenous ZnT8 level increased exponentially with a time constant of 3.7 ± 0.5 h (Fig. 2*E*), but the recovery only reached 75.4% of the endogenous ZnT8 level in untreated EndoC-$\beta$H1 cells. The lack of a full recovery was likely caused by the presence of residual cytokines after switching to the cytokine-free medium. As shown in Fig. 2*C*, the lowest cytokine concentration (0.01×) used in the experiment still induced a solid 19.3% ZnT8 down-regulation, suggesting that a trace amount of residual cytokine could prevent a full recovery. Taken together, cytokines elicited an acute, graded, and reversible ZnT8 down-regulation over a 1,000-fold concentration range.

### *Adaptive cellular responses*

The reversibility of cytokine-induced ZnT8 down-regulation reflected an adaptive cellular response to inflammatory stress. To evaluate the extent of cell damage under different types of stress, we used a DNA-binding fluorescence dye to monitor changes in the cell membrane integrity. 1× Glc + PA and modest zinc exposure (≤200 $\mu$M) did not alter the cell integrity as compared with untreated cells (Fig. 2*F*). Cytokines progressively compromised cell integrity with increasing concentrations. However, normalizing the cytokine-induced fluorescence increase to that of detergent-induced cell lysis indicated that <10% of cells were damaged following a 10× cytokine exposure for 48 h (Fig. 2*F*). A 1× cytokine exposure for 24 h increased the relative CellTox intensity to 5.3% from a background level of the untreated control at 4.1% (Fig. 2*F*). Thus, the cytotoxicity level was negligibly low, consistent with earlier findings that a similar cytokine mixture exposure did not induce proapoptotic markers in EndoC-$\beta$H1 cells (38).

### *Selective ZnT8 targeting*

To further evaluate the effects of metabolic and inflammatory stress on the insulin secretory pathway, we exposed EndoC-$\beta$H1 cells to 1× cytokine or 1× Glc + PA for 24 h and then used immunoblotting to compare protein expression lev-

els with and without the stress exposure. Total cell lysates were probed by antibodies to ZnT8 (mAb20), two ER-resident membrane proteins (BAP31 and calnexin), two ISG-resident membrane proteins (IA2 and VAMP2), and an ER/Golgi membrane protein (TMED3) (39). Three proteins outside of the insulin secretory pathway (α-tubulin, GAD65, and stearoyl-CoA desaturase (SCD)) were analyzed in parallel. Using α-tubulin as an internal control on the same immunoblot, we observed a marked reduction of ZnT8 in cytokine-treated cells but no change in Glc + PA–treated cells (Fig. 3*A*). Of note, mAb20 detected two naturally occurring *SLC30A8* splice variants (40), and their combined intensity was compatible with that of α-tubulin (Fig. 3*A*). Other tested membrane proteins except for IA2 showed no change following either cytokine or metabolic stress (Fig. 3*B*). Cytokine exposure induced an insignificant IA2 reduction as compared with a more pronounced ZnT8 down-regulation (Fig. 3*C*). Two additional proteins, GAD65 and SCD, showed differential responses to cytokine and metabolic stress (Fig. 3*C*, detailed *below*). Moreover, densitometric quantification at different time points of stress exposures showed a time-dependent decline of the endogenous ZnT8 level after cytokine exposure but no difference following metabolic stress up to 48 h (Fig. 3*D*). This immunoblotting result validated independent measurements by ZnT8-ELISA (Fig. 2, *C* and *D*). The α-tubulin and BAP31 levels also remained unchanged under both cytokine and metabolic stress for 48 h (Fig. 3*D*). In β-cells, BAP31, calnexin, TMED3, VAMP2, IA2, and ZnT8 are distributed along the insulin secretory pathway from ER to ISG. Among these proteins, ZnT8 showed the strongest cytokine responsiveness, acting as a selective target of cytokine-induced down-regulation.

### *Localization of ZnT8 to the ER*

Previous work established that ZnT8, IA2, and VAMP2 were localized to ISGs of pancreatic β-cells (41–43). The differentiated response of ZnT8 from that of IA2 and VAMP2 prompted a reevaluation of ZnT8 subcellular localization. Co-immunostaining EndoC-βH1 cells with mAb20 and a rabbit polyclonal antibody to insulin, BAP31, IA2, VAMP2, TMED3, or Golgin-97 revealed two distinct levels of ZnT8 immunofluorescence signals. A lower but broadly distributed intensity appeared co-localized with BAP31 and TMED3 and partly with IA2 and VAMP2 immunofluorescence, whereas a high but confined intensity overlapped the immunofluorescence of insulin and partly IA2 and VAMP2 (Fig. 4, *A–E*). Co-immunostaining ZnT8 and the Golgi marker Golgin-97 suggested no immunofluorescence overlap (Fig. 4*F*). Quantitative analysis gave Manders' split coefficients (MSCs) of 1.00 in respective regions of interest (ROIs) for the protein pairs ZnT8-insulin, ZnT8-BAP31, ZnT8-TMED3, ZnT8-VAMP2, and ZnT8-IA2, whereas the MSC value for the ZnT8-Golgin97 pair was 0.20. Thus, confocal imaging suggested a broad ER localization of endogenous ZnT8 in addition to its high-density clustering associated with ISGs.

We validated the imaging observations by co-immunoprecipitation. Homogeneous liposomes (~100 nm in diameter based on light-scattering measurements) derived from EndoC-βH1 cells were captured by mAb20-PEG5K-Dynabeads. Proteins in proximity to ZnT8 in liposomes were probed by immunoblotting. Dynabeads conjugated with mouse IgG via the same PEG5K linker were used to assess nonspecific liposome capture. The membrane sidedness of the liposomal preparation was ~50% right-side-out and ~50% inside-out. mAb20 on magnetic beads captured right-side-out liposomes, whereas nonspecific liposome binding to IgG-PEK5k-beads was not detected (Fig. 5*A*). Immunoblotting analysis of captured lipo-

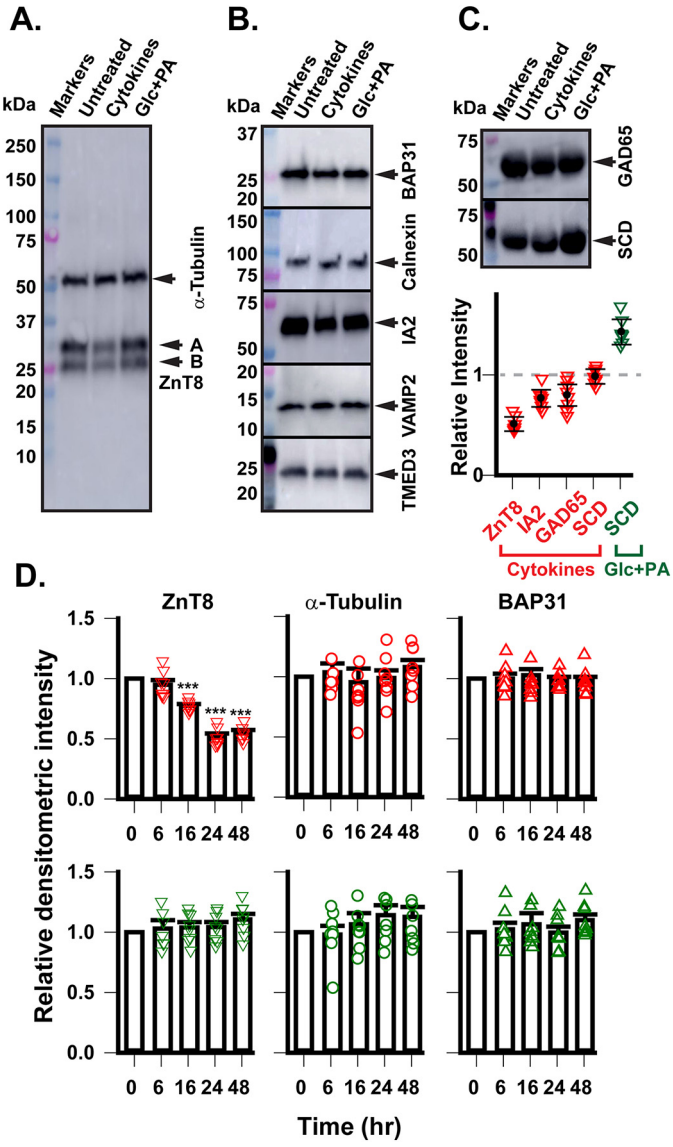


**Figure 3. Effects of cytokine and metabolic stress on proteins in different subcellular locations.** *A*, immunoblotting analysis of total cell lysate from ~$2 \times 10^4$ EndoC-βH1 cells with or without stress exposure as indicated. ZnT8 and α-tubulin were probed with respective antibodies at the same time on the same immunoblot. Two ZnT8 splice variants are marked as *A* and *B*, respectively. *B*, immunoblotting analysis of total cell lysate using antibodies to BAP31, calnexin, IA2, VAMP2, and TMED3 as indicated. *C*, immunoblotting analysis of total cell lysates using antibodies to GAD65 and SCD as indicated (*top*) and responses of four β-cell autoantigens and SCD to cytokine (*red*) or metabolic stress (*green*) as indicated (*bottom*). Respective protein band intensities were quantified and normalized to that of untreated controls on the same immunoblots. *D*, densitometric quantification of ZnT8, α-tubulin, and BAP31 at different time points of cytokine (*red*) and Glc + PA exposures (*green*). Protein band intensities were normalized to that of untreated controls on the same immunoblots. ***, statistical significance by paired *t* test with $p < 0.001$. *Error bars*, S.E. of eight measurements from four independent experiments.

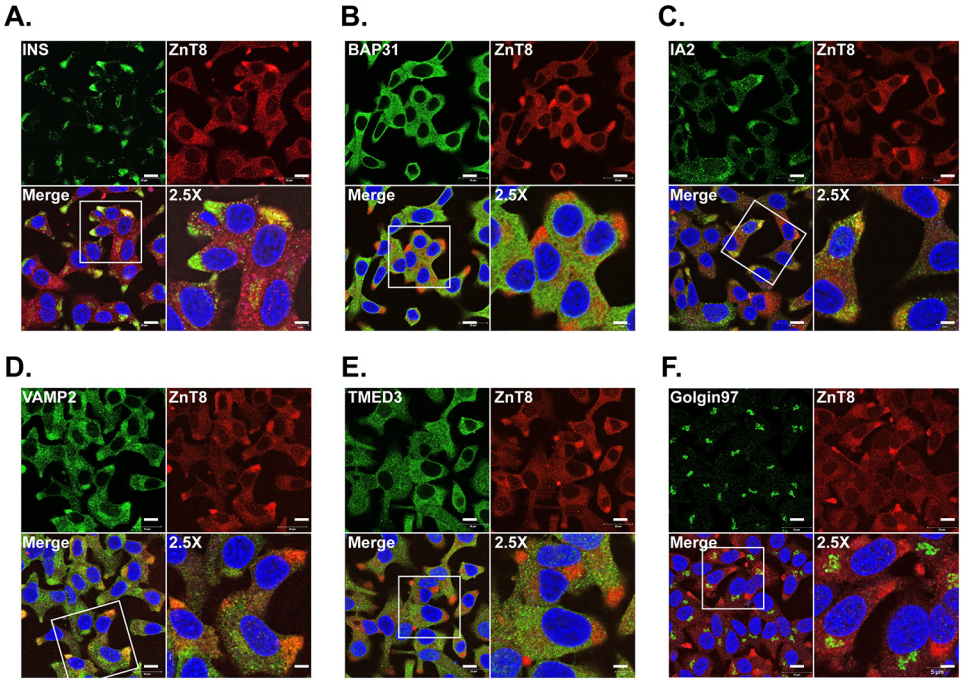


**Figure 4. Confocal microscopy imaging of ZnT8 colocalization with organelle markers in EndoC-βH1 cells.** Cells were immunostained with mouse mAb20 together with a rabbit antibody to insulin (*A*), BAP31 (*B*), IA2 (*C*), VAMP2 (*D*), TEMD3 (*E*), or Golgin97 (*F*) as indicated. The mouse and rabbit primary antibody were visualized by an anti-mouse (*red*) and anti-rabbit (*green*) secondary antibody, respectively. A region of interest in the *merge panel* is *marked* and shown in ×2.5 magnification. *Scale bars*, 10 μm in ×*1* and 4 μm in ×*2.5 panels*.

somes using antibodies to BAP31, IA2, TMED3, or VAMP2 showed that each of these proteins was co-immunoprecipitated with ZnT8. In contrast, Golgin97 was not detected (Fig. 5*B*), in agreement with the confocal imaging results (Fig. 4).

### *Quantification of ER-resident ZnT8*

To estimate the amount of ER-associated ZnT8 relative to the total ZnT8 in EndoC-βH1 cells, we conjugated a polyclonal BAP31 antibody to Dynabeads that could capture >95% BAP31-liposomes because this polyclonal antibody recognized multiple BAP31 epitopes on both sides of the membrane. ZnT8 in the captured BAP31-liposomes was detected on immunoblots by biotinylated mAb20 followed by HRP-conjugated streptavidin. The use of biotinylated mAb20 avoided detection of a small amount of pAb light chains that were partially co-eluted with ZnT8 and detected at a position close to that of ZnT8 on immunoblots. Each ZnT8 protein band on the immunoblot was measured and normalized to the total ZnT8 in the cell lysate. Densitometric quantification showed that 60.4 ± 4% of ZnT8 in the cell lysate was in the flow-through (unbound), whereas 48.7 ± 6% of ZnT8 was captured (bound) by anti-BAP31–conjugated beads (Fig. 5*C*), yielding an estimate of about 50% of cellular ZnT8 associated with ER. Next, we compared the cytokine effects on total and ER-associated ZnT8. Exposing EndoC-βH1 cells to 1× cytokine mixture for ~16 h reduced the total cellular ZnT8 to 66 ± 3% relative to the untreated control (100%) (Fig. 5*D*), in agreement with the results presented in Figs. 2*D* and 3*D*. By comparison, anti-BAP31–conjugated beads captured 55.5 ± 4% of total ZnT8 in untreated cells *versus* 13.8 ± 1% of total ZnT8 in cytokine-treated cells (Fig. 5*D*). The ratio of 13.8/55.4 indicated that cytokine exposure reduced the ER-resident ZnT8 to 24.9% of the pre-exposure level. Compared with a 66% postcytokine level for total cellular ZnT8, cytokines had a more pronounced effect on ER-resident ZnT8. Confocal imaging showed that 1× cytokine exposure for 24 h resulted in a complete loss of ER-associated ZnT8 immunofluorescence, whereas the ISG-associated signal remained largely unchanged (Fig. 5*E*), further indicating that ER was the primary site of cytokine-induced ZnT8 down-regulation.

### *Response of HLA-I molecules*

Because the endogenous levels of BAP31, calnexin, TMED3, VAMP2, and IA2 showed no or insignificant responsiveness to stress exposures, we further examined stress-induced perturbation of two additional proteins, HLA-I molecules (44) and insulin (45). Exposing EndoC-βH1 cells to 1× cytokine mixture for 24 h sharply activated HLA-I expression over a low background of untreated cells, whereas 1× Glc + PA exposure did not affect the HLA-I expression level (Fig. 6*A*). The ZnT8 level on the same immunoblot was reduced by ~50% concurrently with a 13.4-fold increase in HLA-I expression, demonstrating a bidirectional response of EndoC-βH1 cells to cytokine stimulation (Fig. 6*A*). A high signal-to-noise ratio of the HLA-I signal on the immunoblot allowed for in-cell HLA-I ELISA quantification using the commercial HLA-I antibody. A marked HLA-I activation was observed for all concentrations down to 0.01× cytokines (Fig. 6*B*). Compared with ZnT8 down-regulation in response to identical cytokine exposures (Fig. 2*C*), linear regression analysis showed a negative correlation between activation of HLA-I molecules and ZnT8 down-regulation ($r^2$ = 0.77; Fig. 6*C*), suggesting that peptides derived from ZnT8 degradation may contribute to HLA-I loading.

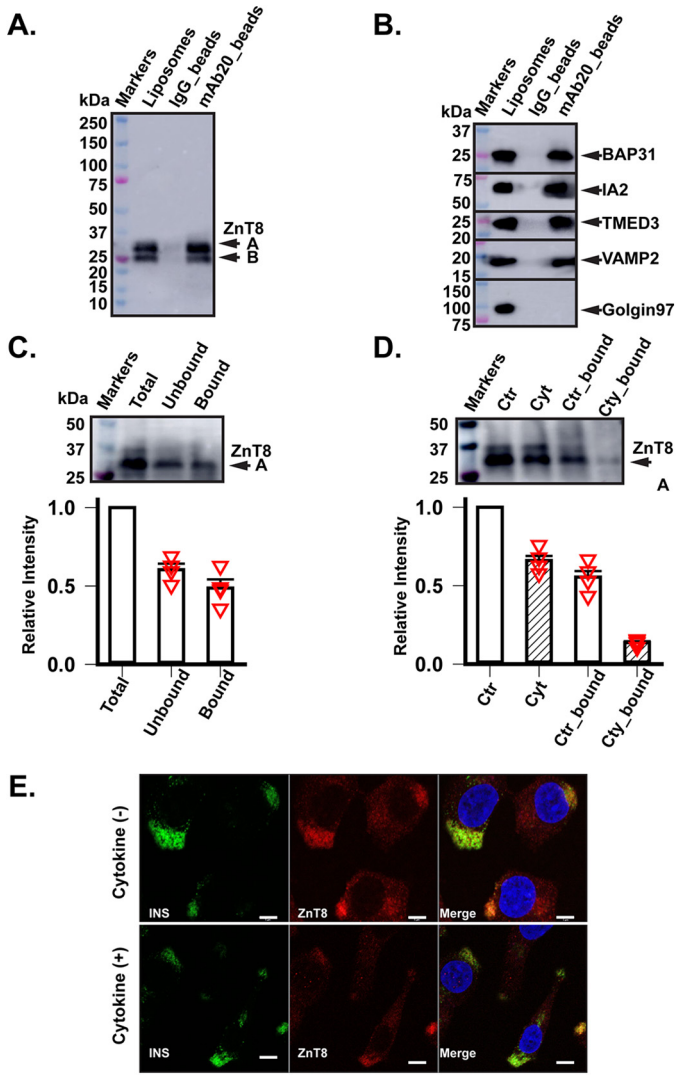


**Figure 5. Co-immunoprecipitation and quantification of ZnT8.** *A*, ZnT8 probed by mAb20 immunoblotting using liposomes from $1 \times 10^6$ cells before and after they were bound to mAb20- or IgG-beads followed by SDS elution. *B*, co-immunoprecipitation of ZnT8 and organelle markers. ZnT8-liposomes were captured by mAb20 beads, eluted, and then probed by an antibody to BAP31, IA2, TMED3, VAMP2, or Golgin97 as indicated. Prebound liposomes and IgG-bead bound liposomes were used as a positive and negative control, respectively. Of note, gel loading of prebound liposomes was half of the mAb20-bead–bound liposomes. *C*, quantification of ER-resident ZnT8. *Top*, representative mAb20 immunoblotting of liposomes before and after incubation with anti-BAP31-beads. Liposomes in the flow-through and SDS-elution of BAP31-beads are *marked* as *unbound* and *bound*, respectively. *Bottom*, densitometric quantification of ZnT8 intensity of total liposomes and unbound and bound fractions. ZnT8 intensities were normalized to the intensity of total liposomes on the same immunoblot. *Error bars*, S.E. of four independent experiments. *D*, cytokine-induced reduction of ER-resident ZnT8. *Top*, a representative mAb20 immunoblotting of liposomes from an equal number of EndoC-$\beta$H1 cells ($1 \times 10^6$). *Ctr* and *Cyt*, liposomes from untreated control and cytokine-treated cells, respectively. Ctr-bound and Cyt-bound are captured Ctr- and Cyt-liposomes on anti-BAP31-beads with SDS elution. *Bottom*, densitometric quantification of ZnT8 intensities with normalization to the Ctr intensity on the same immunoblot. *Error bars*, S.E. from four independent experiments. *E*, confocal microscopy imaging of EndoC-$\beta$H1 cells with and without exposure to 1× cytokine mixture for 24 h, which were then co-immunostained with mouse mAb20 and a rabbit anti-insulin pAb. *Scale bars*, 5 $\mu$m.

### *Insulin response*

To measure insulin responses to metabolic, zinc, and cytokine stress, we exposed EndoC-$\beta$H1 cells to different stress conditions for 24 h as described in the legend to Fig. 2 and then quantified insulin secretion in response to 20 mM Glc plus 45 $\mu$M isobutylmethylxanthine (a GSIS enhancer) using a commercial insulin assay based on homogeneous time-resolved fluorescence (46). None of the stressors induced a significant change in GSIS (Fig. 7*A*). By comparison, total insulin contents under different stress conditions exhibited distinct dose-dependent profiles (Fig. 7*B*). Increasing the Glc + PA concentration progressively increased the cellular insulin content in a quasi-linear fashion except for the highest concentration that might approach onset of glucolipotoxicity. Increasing the zinc concentration also increased the insulin content until the concentration reached 600 $\mu$M, where zinc toxicity was evident (Fig. 2*F*). Finally, increasing the cytokine concentration induced a monophasic decline of the insulin content to 60% of the untreated control.

### *Cytokine-permissive ZnT8-insulin correlation*

The distinct dose profiles of insulin responses suggested that the type and dosage of stressor may determine the relationship between ZnT8 expression and insulin production. We quantified such relationships by linear regression analysis of ZnT8 and insulin dose responses. Glc + PA exposures altered insulin production (Fig. 7*B*), but not ZnT8 expression (Fig. 2*A*), yielding a low $r^2$ value of 0.48 (Fig. 7*C*). Extracellular zinc exposures altered both endogenous ZnT8 (Fig. 2*B*) and insulin levels (Fig. 7*B*), but regression analysis yielded an $r^2$ value of 0.04 (Fig. 7*C*), indicating a lack of ZnT8-insulin correlation. In contrast, cytokine exposures yielded a striking correlation between ZnT8 (Fig. 2*C*) and insulin (Fig. 7*B*) levels with an $r^2$ value of 1.00 (Fig. 7*C*). Hence, our experiments identified cytokine exposure as a permissive condition for a cross-talk between down-regulations of ZnT8 expression and insulin production in a highly coordinated manner.

### *Molecular underpinnings for differential ZnT8 responses to metabolic and cytokine stress*

The lack of ZnT8-insulin correlation under metabolic stress (Fig. 7*C*) suggested a disconnection of ZnT8 from the regulatory pathway linking metabolic stress to insulin expression. Signaling pathways evoked by metabolic and inflammatory stress are thought to be different (47, 48), namely an NF-$\kappa$B independent mechanism for FFA and an NF-$\kappa$B dependent mechanism for cytokines (49). Proteomic profiling of rat INS-1 cells before and after acute high PA or Glc + PA exposures revealed a global up-regulation of desaturase expression (50), contributing to adaptive FFA detoxification by converting the lipotoxic FAAs to the protective unsaturated species (21, 51). Accordingly, we used SCD as a marker to demonstrate differential stress responses of EndoC-$\beta$H1 cells. Anti-SCD immunoblotting showed that SCD expression was up-regulated by high Glc + PA exposure but irresponsive to cytokine stress (Fig. 3*C*). By comparison, the ZnT8 expression was irresponsive to high Glc + PA exposure but down-regulated by cytokine stress (Fig. 3*D*). The differential responses of ZnT8 and SCD validated the divergence of metabolic and cytokine signaling pathways in EndoC-$\beta$H1 cells.

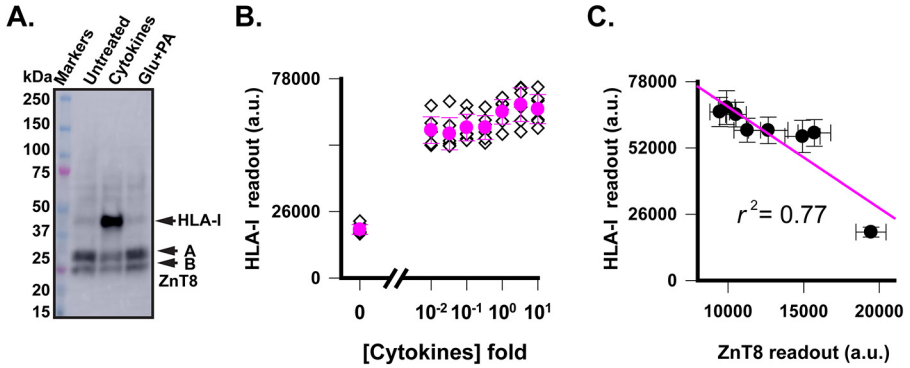


**Figure 6. Responses of HLA-I molecules to metabolic and cytokine stress.** *A*, anti-HLA-I immunoblot analysis of cell lysates of EndoC-βH1 cells with cytokine and metabolic pre-exposures as indicated. ZnT8 on the same immunoblot was probed with mAb20 as a reference. *B*, dose-dependent response of HLA-I molecules to cytokine exposures. *Filled circles* and *error bars*, means and S.D. of eight replicated measurements (*diamonds*) by HLA-I ELISA. *C*, correlation of endogenous ZnT8 and HLA-I expression. Data points (*filled circles*) were taken from Fig. 2*C* and *panel B* for endogenous ZnT8 and HLA-I levels over a range of identical cytokine concentrations. *Error bars*, S.D.; *solid line*, linear regression ($r^2 = 0.77$). *a.u.*, arbitrary units.

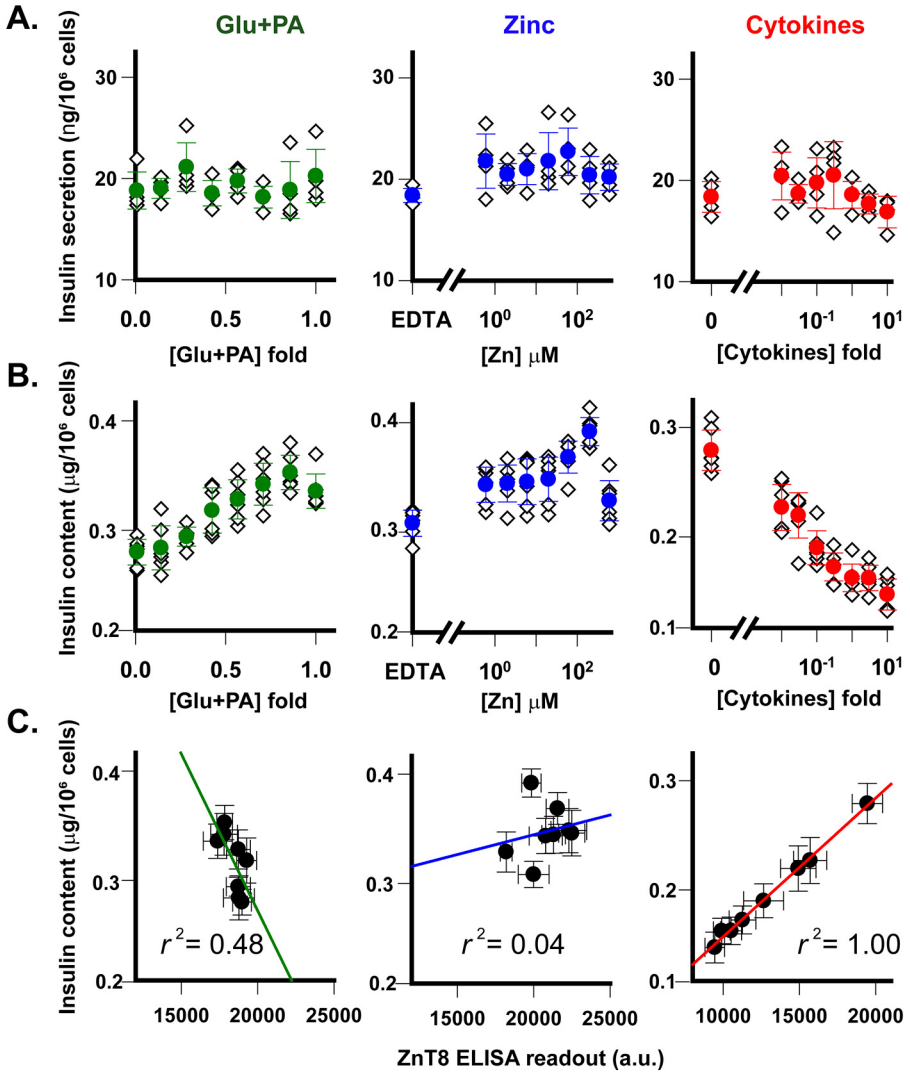


**Figure 7. Dose responses of insulin secretion and production and their correlations with ZnT8 expression under different stress conditions.** *A*, GSIS from EndoC-βH1 cells that were pre-exposed to different concentrations of Glc + PA (*green*), zinc (*blue*), and cytokines (*red*) for 24 h. *Filled circles* and *error bars*, means and S.D. of eight replicated measurements (*diamonds*). *B*, insulin content in EndoC-βH1 cells under identical stress exposures as in *A*. *C*, correlations of ZnT8 expression and insulin production under different stress conditions. Data points were generated using the endogenous ZnT8 levels from Fig. 2 (*A–C*) and insulin contents from *B* measured under identical stress exposures. *Solid lines*, linear regressions; the levels of ZnT8-insulin correlation are indicated by respective $r^2$ values.

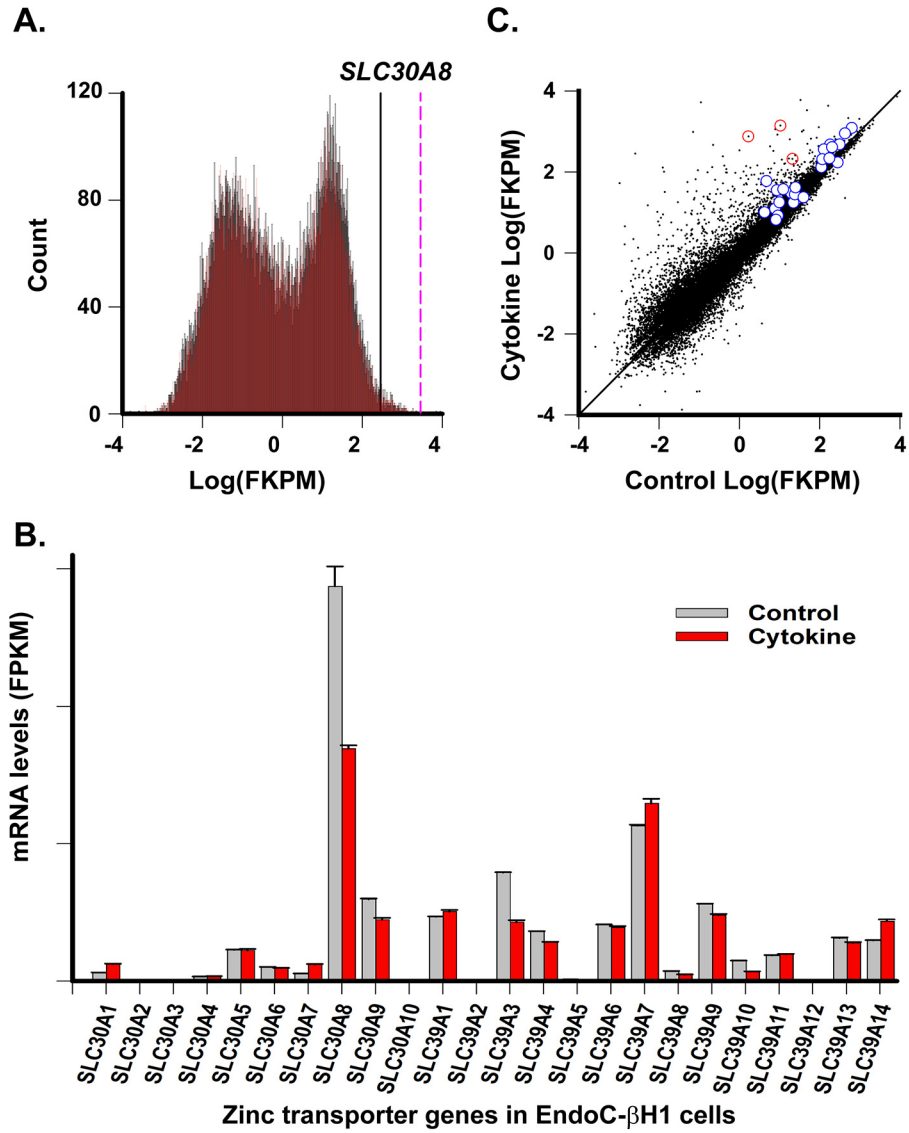


**Figure 8. Transcriptomic analysis of EndoC-βH1 cells in response to cytokine exposure.** *A*, overlap of distributions of mRNA levels in the EndoC-βH1 transcriptome with (*red*) or without (*black*) 1× cytokine exposure for 24 h. *Black line*, *SLC30A8* mRNA level in EndoC-βH cells. *Dashed magenta line*, a 10-fold increase of the *SLC30A8* mRNA level in human pancreatic β-cells (83). *B*, mRNA levels of *ZnT* (*SLC30*) and *ZIP* (*SLC39*) gene families in EndoC-βH1 cells. *Error bars*, S.D. of three biological replicates. *C*, correlation of mRNA levels with and without cytokine exposure along a *diagonal line*. *Off-diagonal data points*, cytokine-induced transcriptional changes. *Red data points*, *LMP2, LMP7*, and *MECl-1* transcripts. *Blue data points*, other UPR-related transcripts listed in Table 1.

### *Immunoproteasome-mediated co-degradations of ZnT8 and insulin*

To illuminate the molecular events leading to parallel down-regulations of ZnT8 and insulin in response to cytokine exposure, we performed Illumina deep sequencing of EndoC-βH1 cells with or without 1× cytokine exposure for 24 h. About 100 million (2 × 100 bp) paired reads per sample were obtained. Mapping these reads to the human genome (build hg38) identified about 44,000 transcripts per sample. Approximately 600 known genes showed differential expression based on the following criteria: a log fold change ≥ 1.5, at least one of the fragments per kilobase of transcript per million (FPKM) ≥ 2, and a $p$ value < 0.05. Cytokine exposure did not alter the overall transcription profile (Fig. 8*A*). The *SLC30A8* mRNA level was within the top 1% of the transcriptome (Fig. 8*A*) and showed the largest fold change among all zinc transporters in EndoC-βH1 cells (Fig. 8*B*). Two ER-resident UPR sensors, inositol-requiring enzyme 1 (IRE1) and PKR-like ER kinase (PERK), were up-regulated by cytokine exposure. Another UPR sensor, activating transcription factor 6 (ATF6), was slightly suppressed, but the ATF6-associated CREB3 sensor was up-regulated (Table 1). Thus, all three branches of the UPR were engaged in cytokine stress (52). In support of this notion, ER chaperones (BIP, CANX, and CALR), protein-disulfide isomerases (PDIA3, -4, and -6), and key transcription factors involved in adaptive UPR signaling (XBP1 and ATF4) were all significantly up-regulated (Table 1). The NF-κB inflammatory signaling pathway was activated as expected for cytokine stimulations, but key components of the apoptotic program (53), c-Jun N-terminal kinase, CHOP, and caspases, remained either unchanged or at a low level (FPKM < 60) with an apparently significant fold increase (Table 1). In contrast, genes in the ER-associated protein deg-

**Table 1**
**Cytokine-induced differential gene expression as determined by RNA-Seq**
Results are mean ± S.D. for three independent measurements.

| Gene | Control (FKPM) | Cytokine (FKPM) | -Fold change | Protein function |
|---|---|---|---|---|
| *SLC30A8* | 287.2 ± 10.4 | 169.1 ± 3.0 | 0.6 | ZnT8, ISG/ER zinc sequestration |
| *SLC39A7* | 113.0 ± 2.4 | 129.3 ± 4.1 | 1.1 | ZIP7, ER/Golgi zinc release |
| *INS + read-throughs* | 30,768.8 ± 1,367.6 | 24,920.6 ± 688.2 | 0.8 | Insulin, ISG |
| *IRE1* | 4.3 ± 0.2 | 9.9 ± 0.2 | 2.3 | UPR sensor |
| *PERK* | 7.9 ± 0.5 | 12.1 ± 1.3 | 1.5 | UPR sensor |
| *ATF6* | 9.3 ± 0.4 | 8.2 ± 0.1 | 0.9 | UPR sensor |
| *CREB3* | 19.9 ± 0.2 | 29.7 ± 0.9 | 1.5 | ATF6-assocated UPR sensor |
| *BIP* | 186.3 ± 5.0 | 466.8 ± 8.1 | 2.5 | ER chaperone protein |
| *CANX* | 321.6 ± 13.4 | 469.9 ± 27.1 | 1.5 | ER chaperone protein |
| *CALR* | 647.1 ± 12.9 | 1,201.0 ± 14.5 | 1.9 | ER chaperone protein |
| *PDIA3* | 438.2 ± 8.4 | 882.3 ± 1.8 | 2.0 | Protein-disulfide isomerase |
| *PDIA4* | 130.5 ± 2.5 | 353.9 ± 6.7 | 2.7 | Protein-disulfide isomerase |
| *PGIA6* | 208.2 ± 1.9 | 403.2 ± 1.8 | 1.9 | Protein-disulfide isomerase |
| *XBP1* | 119.4 ± 1.0 | 203.2 ± 1.5 | 1.7 | Adaptive UPR kinase |
| *ATF4* | 178.8 ± 5.2 | 214.4 ± 0.1 | 1.2 | Adaptive UPR kinase |
| *NFKB1* | 10.1 ± 0.4 | 17.5 ± 0.5 | 1.7 | Proinflammatory signaling kinase |
| *NFKB2* | 8.7 ± 0.5 | 34.9 ± 0.2 | 4.0 | Proinflammatory signaling kinase |
| *MAPK8* (*JNK1*) | 26.6 ± 0.9 | 20.9 ± 0.5 | 0.8 | Proapoptotic UPR kinase |
| *MAPK9* (*JNK2*) | 22.6 ± 0.6 | 17.2 ± 0.4 | 0.8 | Proapoptotic UPR kinase |
| *MAPK10* (*JNK3*) | 24.6 ± 0.8 | 27.3 ± 0.9 | 1.1 | Proapoptotic UPR kinase |
| *CHOP* (*DDIT3*) | 12.6 ± 0.6 | 36.7 ± 1.9 | 2.9 | Proapoptotic UPR kinase |
| *CASP2* | 40.3 ± 0.18 | 23.2 ± 0.6 | 0.6 | Proapoptotic caspase cascade |
| *CASP3* | 25.5 ± 0.5 | 40.8 ± 0.5 | 1.6 | Proapoptotic caspase cascade |
| *CASP4* | 4.8 ± 0.4 | 58.6 ± 3.2 | 12.2 | Proapoptotic caspase cascade |
| *CASP9* | 8.3 ± 0.4 | 6.5 ± 0.6 | 0.8 | Proapoptotic caspase cascade |
| *PSMB8* | 10.7 ± 0.3 | 1,371.2 ± 16.6 | 128.1 | ERADE, immunoproteasomes, LMP7 |
| *PSMB9* | 1.7 ± 0.2 | 742.1 ± 7.9 | 436.5 | ERADE, immunoproteasomes, LMP2 |
| *PSMB10* | 21.4 ± 1.4 | 205.8 ± 2.1 | 9.6 | ERADE, immunoproteasomes, MECl-1 |

radation (ERAD) pathway were sharply activated, including *LMP2*, *LMP7*, and *MECl-1*, which encoded three catalytic subunits of immunoproteasomes with a 436.5-, 128.1-, and 9.6-fold increase, respectively (Table 1). These immunoproteasome components were distinctly positioned off-diagonal in a linear correlation of EndoC-βH1 transcriptomes with and without cytokine exposure, indicating a prominent cytokine-induced activation of ERAD (Fig. 8*C*).

The proteolytic activities of LMP2, LMP7, and MECl-1 are essential to generating antigenic peptides with a hydrophobic C terminus for proper HLA-I loading (54). ZnT8 and insulin are two major β-cell autoantigens susceptible to immunoproteasome digestion and HLA-I presentation on pancreatic β-cells (10, 55–58). A dramatic increase of the HLA-I protein level and its negative correlation with the endogenous ZnT8 level (or positive correlation with ZnT8 degradation) (Fig. 6*C*) suggested that immunoproteasome may mediate cytokine-induced ZnT8 ERAD for HLA-I loading. To test this hypothesis, we used a membrane-permeable natural product epoxomicin to specifically inhibit LMP7 and MECL-1 (59). Exposing EndoC-βH1 cells to epoxomicin blocked cytokine-induced down-regulations of both ZnT8 and insulin (Fig. 9*A*), indicating a shared immunoproteasome-mediated ERAD pathway for ZnT8 and insulin degradation. Epoxomicin alone neither altered ZnT8 expression nor affected cell viability (Fig. 9, *A* and *B*). However, a combination of epoxomicin and 1× cytokine triggered apoptosis, resulting in 26.8% damaged cells following a 24-h exposure (Fig. 9*B*).

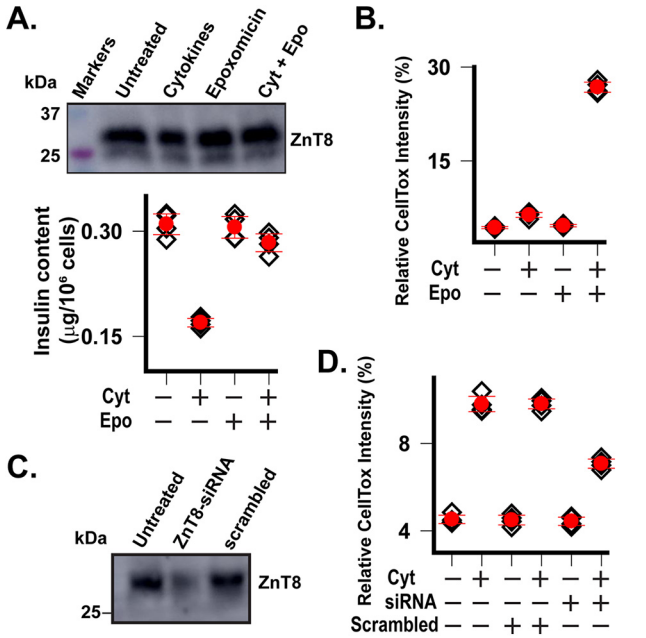


**Figure 9. Inhibition of ZnT8 and insulin degradation and cytoprotection by *ZnT8* knockdown.** *A*, anti-ZnT8 immunoblotting of EndoC-βH1 cells following a 24-h exposure to 1× cytokines or 1 μM epoxomicin in various combinations as indicated (*top*), cellular insulin contents measured in parallel (*bottom*). *B*, normalized CellTox fluorescence intensities in response to 1× cytokines or 1 μM epoxomicin in various combinations as indicated. *C*, anti-ZnT8 immunoblotting of EndoC-βH1 cells treated with ZnT8-targeting or scrambled siRNA as indicated. *D*, normalized CellTox fluorescence intensities in response to 15× cytokine exposure for 24 h. EndoC-βH1 cells were pretreated with ZnT8-targeting or scrambled siRNA as indicated. *Error bars*, S.D. of four independent measurements.

### *ZnT8 knockdown reduced cytokine-induced cell damage*

The proapoptotic effect of the combined actions of epoxomicin and cytokine suggested that a blockade of immunoproteasome-mediated ZnT8 degradation triggered a transition from adaptive to proapoptotic UPR under cytokine stress. This finding raised the possibility that reducing the ZnT8 ER burden may promote adaptive UPR response. To test this hypothesis,

we used siRNA to reduce the cellular ZnT8 level and monitored cytokine-induced loss of cell integrity by the CellTox fluorescence assay. Transfection of EndoC-βH1 cells with ZnT8-targeting siRNAs caused a ~70% reduction in the ZnT8 protein level, whereas scrambled siRNA had no effect (Fig. 9*C*). *ZnT8* knockdown markedly reduced cell damage induced by 15× cytokine exposures for 24 h (Fig. 9*D*), demonstrating that ZnT8 knockdown significantly attenuated cytokine cytotoxicity.

## Discussion

ZnT8 is generally thought to be a simple zinc transporter performing a zinc enrichment role in ISGs. Our results indicate that ZnT8 is temporally and spatially regulated to modulate zinc, ER, and insulin homeostasis. Our recent findings also showed that GSIS promotes ZnT8 trafficking to the surface membrane (60), where ZnT8 becomes a surface autoantigen recognized by autoantibodies that arise from autoimmunity in T1D (33, 61). Hence, emerging evidence suggests cross-talk among multiple regulatory pathways intersecting at ZnT8. The current research paradigm based on *SLC30A8* deletion/overexpression carries a significant liability to experimental artifacts due to drastic perturbation of a multitude of signaling pathways. The mAb20-based in-cell ZnT8 assay allows for tracking fluctuations of endogenous ZnT8 levels, establishing ZnT8 as a major cytokine-responsive UPR client protein in the ER.

*SLC30A8* is highly expressed in human pancreatic β-cells (Figs. 3*A* and 8*A*), imposing a significant ER burden that is also under pressure of high demand on insulin production and secretion. Cytokine exposure may further render β-cells susceptible to accumulation of misfolded proteins, exacerbating ER stress (45). Our experiments showed that human β-cells responded to acute cytokine exposure with a rapid, graded, and reversible down-regulation of the cellular ZnT8 level. These findings are consistent with earlier studies of cytokine-regulated *SLC30A8* expression in rodent β-cells with some differences in the effects on GSIS and the cellular insulin content (62–64). We found that cytokine-induced ZnT8 down-regulation did not affect GSIS in human insulinoma cells but strongly correlated with the insulin content. The coupled down-regulations of ZnT8 and insulin provide direct evidence for UPR converging on two major ER burdens, highlighting the importance of ZnT8 and insulin decongestion in restoring ER homeostasis under inflammatory insult. In support of this notion, blocking ZnT8 degradation by an immunoproteasome inhibitor accelerated cell death, whereas facilitating ZnT8 down-regulation by siRNA knockdown protected cells against cytokine cytotoxicity (Fig. 9, *B* and *D*). These results are in line with a previous finding that *SLC30A8* overexpression potentiated IL-1β induced apoptosis of rat pancreatic β-cells (63). Human genetics data and functional studies of ZnT8 polymorphic variants provided further support for a pathogenic effect of ZnT8 up-regulation. A nonsynonymous polymorphic variant of ZnT8 (R325) has a higher zinc transport activity (34, 65) and thermostability (66), and this polymorphism is associated with a higher T2D risk (11). This causal relationship is further validated by a recent whole-exome sequencing analysis targeting all of the coding sequences in the human genome (67).

The responsiveness of ER-resident ZnT8 to cytokine stimulations may also contribute to restoring zinc homeostasis in ER, which has an enriched luminal concentration (≥5 nM) over a low cytosolic zinc level (0.1–1 nM) (68). Among all zinc transporters in EndoC-βH1 cells, *SLC39A7* is the second-highest transcribed gene after *SLC30A8* and also has a significant cytokine response at the mRNA level (Fig. 8*B*). *SLC39A7* encodes a major zinc-release transporter ZIP7 in the ER (69, 70). The reduction of the *SLC30A8* transcript appears functionally synergetic with an increase of *SLC39A7* because ZnT8 and ZIP7 transport zinc in opposite directions across the ER membrane (5, 6). ZIP7 up-regulations were found to attenuate ER stress in MG-63 osteosarcoma cells, intestinal epithelial cells, and embryonic rat heart–derived cells (H9c2) (71–73). Likewise, cytokine-induced ZnT8 down-regulation may attenuate ER stress by reducing the ER zinc content, which may be tuned to a reduced demand on zinc for proinsulin loading. Hence, a coupling between ZnT8 expression and insulin production may be of physiological significance for the zinc-dependent process of proinsulin folding and processing (74).

Understanding how cellular ZnT8 responds to disease-driving stress is the first step toward understanding the role of ZnT8 in T2D pathogenesis. Our experiments reveal differential ZnT8 responses to metabolic and inflammatory stress and establish a novel immunologic connection between cytokine-induced ZnT8 down-regulation and β-cell adaptive UPR through immunoproteasome-mediated co-degradation of two major β-cell autoantigens. Autoantibodies to ZnT8 or insulin, together with two additional autoantigens, IA2 and GAD65, were found in ~94% of patients with T1D (75). Whereas these autoantigens are believed not to activate cytotoxic T-cells in T2D, our results revealed selective cytokine susceptibilities of ZnT8 and insulin over IA2 and GAD65 (Fig. 3*C*). A robust cytokine-induced ZnT8 and insulin down-regulation at a concentration 1,000-fold below the cytotoxicity level (Figs. 2*C* and 7*B*) suggests a functional relevance to chronic activation of the innate immune system associated with obesity (25).

Besides being a possible player in obesity-driven low-grade inflammation that predisposes individuals to develop T2D, ZnT8 as a major autoantigen elicits both humoral and cellular autoimmunity in the development of T1D (9, 10, 76, 77). Hence, the pathogenesis of T1D and T2D appears to intersect at ZnT8, which confers immune susceptibility. There is a growing appreciation that β-cell sensitivity to stress may contribute to the risk of developing both T1D and T2D (78). The identification of ZnT8 as a cytokine-responsive ER burden links β-cell inflammation to ER stress, whereas the protective effect of ZnT8 down-regulation for inflamed β-cells suggests a potential therapeutic strategy to mimic the natural protection of *SLC30A8* haploinsufficiency found in humans with lower T2D risk (12). A caveat to increasing β-cell resilience by ZnT8 down-regulation is a parallel down-regulation of insulin production (Fig. 7*C*), potentially leading to a loss of insulin secretory capacity under prolonged and severe inflammatory exposure. Further research is needed to develop a strategy to modulate the ZnT8 level to balance β-cell survival and insulin production in inflamed pancreatic islets.

## Experimental procedures

### *Reagents*

Reagent mAb20 was validated as described previously (33). Antibody-conjugated Dynabeads for biomagnetic separations were prepared using *N*-hydroxylsuccinimide (NHS) functionalized PEG NHS-PEG5K-NHS (Nanocs, catalog no. PG2-NS-5k) to cross-link antibodies with surface-reactive amine groups on 2.8-$\mu$m hydrophilic M-270 Amine-Dynabeads (Invitrogen, catalog no. 14307D). A 50-fold molar excess of NHS-PEG5K-NHS over the surface primary amine groups was used for bead activation and 5-fold molar excess of mAb20, mouse-IgG, or anti-BAP31 polyclonal antibodies (Proteintech, catalog no. 11200-1-AP) yielded an antibody surface coating density of ~100 $\mu$g of antibody per ml of beads.

### *Cell cultures*

EndoC-$\beta$H1 cells from Univercell-Biosolutions had a doubling time of ~7–10 days. Cells (passage between 40 and 60) were detached from culture flasks using 0.05% trypsin and 0.53 mM EDTA and then reseeded at 75,000 cells/well at 70% confluence in a 96-well TPP plate (Sigma, catalog no. Z707902) coated with Matrigel-fibronectin matrix as described (79). The cells were subcultured at 37 °C in a 5% $CO_2$ humidified atmosphere and grown in a serum-free culture medium containing 11 mM glucose Dulbecco's modified Eagle's medium (Thermo Fisher Scientific, catalog no. 11885076), 2% BSA faction V (Sigma, catalog no. 10735078001), 10 mM nicotinamide (Sigma, catalog no. 47865-U), 50 $\mu$M 2-mercaptoethanol (Thermo Fisher Scientific, catalog no. 21985-023), 5.5 $\mu$g/ml transferrin (Sigma, catalog no. T8158-100 mg), 6.7 ng/ml sodium selenite (Sigma, catalog no. S5261-25g), 100 units/ml penicillin, and 100 $\mu$g/ml streptomycin (Thermo Fisher Scientific, catalog no. 15140122). Flp-In, T-Rex-HEK293 cells with or without doxycycline-induced ZnT8 overexpression were generated and cultured as described preciously (34).

### *Stressor exposures*

PA-BSA conjugation was prepared by adding PA powder to a final concertation of 8 mM in 1.6 mM FFA-free BSA (Sigma, catalog no. A7030-50G) predissolved in 135 mM NaCl, 3.6 mM KCl, 0.5 mM $MgCl_2$, and 10 mM HEPES (pH 7.4). The mixture was incubated with gentle stirring at 37 °C and then filter-sterilized and stored at 4 °C as described previously (80). When added to the cell culture, the PA-BSA mixture was diluted 13.3-fold with a supplement of glucose to make a 1× Glc + PA solution containing 0.6 mM PA and 48 mM Glc. A cytokine mixture was prepared before each experiment by mixing individual stock solutions of IL-1$\beta$, IFN-$\gamma$, IL-17, and TNF$\alpha$ at the respective concentrations used previously on human islets and EndoC-$\beta$H1 cells (37). 1× cytokine mixture in the culture medium contained 5 ng/ml IL-1$\beta$, 10 ng/ml TNF$\alpha$, 50 ng/ml IFN-$\gamma$, and 100 ng/ml IL-17. All cytokines were provided by R&D Systems (Minneapolis, MN). The subcultured EndoC-$\beta$H1 cells were allowed to adhere for 24 h prior to the addition of experimental media containing Glc + PA, zinc, or cytokine mixture in serial dilutions with eight replicates. After a designated exposure period, the endogenous ZnT8 level in each well was analyzed along with stress-induced cytotoxicity, GSIS and cellular insulin content. For cytokine withdrawal experiments, cells were first exposed to 1× cytokine for 24 h and then cultured in the cytokine-free culture medium for different recovery periods before analysis.

### *In-cell ELISAs*

EndoC-$\beta$H1 cells in a 96-well plate with or without stressor exposures were fixed in 50 $\mu$l/well Flow Cytometry Fixation Buffer (R&D Systems, catalog no. FC004) and then permeabilized in Permeabilization/Wash Buffer I (R&D Systems, catalog no. FC005) for 1 h with 2.5% BSA as a blocking reagent. Next, mAb20 or a rabbit anti-HLA-I antibody (Proteintech, catalog no. 15240-1-AP) was 1:600 or 1:60 diluted to Permeabilization/Wash Buffer I plus 0.5% BSA. Cells in each well were incubated with the diluted antibody solution for 2 h at 37 °C, washed once, and then exposed to an HRP-conjugated anti-mouse IgG (H+L) (Invitrogen, catalog no. 62-6520) or anti-rabbit IgG (H+L) antibody (Invitrogen, catalog no. 62-6120) in a 1:3000 dilution in Permeabilization/Wash Buffer I plus 0.1% BSA. After a 1-h incubation with the secondary antibody at room temperature, cells were washed three times to remove unbound antibodies before adding SuperSignal ELISA Femto Substrate (Thermo Fisher Scientific, catalog no. 37075). The HRP reaction was terminated at 5 min by transferring the reaction mixture to a 96-well opaque microplate for chemiluminescence quantification on a FlexStation-3 multimode microplate reader.

### *Cytotoxicity assay*

Cell culture and experiments were performed in a 96-well plate in culture media without phenol red (Sigma, catalog no. D4947). Cytotoxicity in cell culture after experimental manipulation was continuously monitored based on the change in the fluorescence intensity of a CellTox green dye (Promega, catalog no. G8741) that preferentially stained dead cells with a loss of membrane integrity. The dye was 1:1,000 diluted in the culture medium and delivered directly to cells at the same time of dose titrations of Glc + PA, zinc, and cytokines. CellTox fluorescence signals were recorded on a FlexStation-3 multimode microplate reader with eight replicates at 0, 1, 2, 4, 6, 8, 20, 24, 30, and 48 h following dye and stressor additions. Viable cells in the control cell culture medium produced no appreciable increases in CellTox fluorescence due to an excellent tolerance of EndoC-$\beta$H1 cells to the dye. At the end of the experiment, all cells were lysed by adding detergent (dodecyl maltoside) to 0.1% in each well, and the maximum CellTox fluorescence intensity was recorded and used for normalization of the CellTox fluorescence intensity.

### *Immunoblotting*

Cells in a 96-well plate were directly resuspended in 50 $\mu$l/well 1× Laemmli Sample Buffer (Bio-Rad, catalog no. 1610737). An aliquot of 15 $\mu$l of SDS-lysate was loaded onto a precast protein gel for SDS-PAGE and subsequent immunoblotting using the following antibodies directed to ZnT8 (mAb20), tubulin (Invitrogen, catalog no. MA1-83256), calnexin (Proteintech, catalog no. 10427-2-AP), BAP31 (Protein-

tech, catalog no. 11200-1-AP), IA2 (Proteintech, catalog no. 10584-1-AP), TMED3 (Proteintech, catalog no. 21902-1-AP), VAMP2 (Proteintech, catalog no. 10135-1-AP), Golgin97 (Proteintech, catalog no. 12640-1-AP), and HLA-I (Proteintech, catalog no. 15240-1-AP). Protein band intensity was measured using ImageJ, and the numerical value for each stressor-treated protein sample was normalized to the untreated sample on the same immunoblot.

### *Immunofluorescence staining, imaging, and colocalization analysis*

EndoC-$\beta$H1 cells were grown on coverslips at 50% confluence, fixed (R&D Systems, catalog no. FC004), permeabilized (R&D Systems, catalog no. FC005), and co-stained with mAb20 at a 1:600 dilution from a 1 mg/ml mAb stock with one of the following antibodies at a 1:50 dilution: anti-insulin antibody allophycocyanin-conjugated (R&D Systems, catalog no. IC1417A) rabbit anti-BAP31, IA2, TMED3, VAMP2, and Golgin97, as described above. Secondary anti-mouse IgG (H+L) conjugated with Alexa Fluor 594 (Invitrogen, catalog no. A11032, dilution 1:1,000), anti-rabbit IgG (H+L) conjugated with Alexa Fluor 647 (Life Technologies, Inc., catalog no. A21244, dilution 1:1,000), and 4′,6-diamidino-2-phenylindole were used for fluorescence imaging on a Zeiss LSM 700 inverted confocal microscope with a ×63 oil objective. ImageJ with an intensity correlation analysis plugin was used to quantify colocalization of ZnT8 immunofluorescence (red channel) and an ER or ISG marker immunofluorescence (green channel) (81). Confocal images were split into red and green channels without background corrections. ROIs were selected for ER or ISG regions, where all pixels above an autothreshold were used to calculate MSCs for red to green channel.

### *Liposome preparation*

EndoC-$\beta$H1 cells at 90% confluence from a 10-cm culture disk with or without 1× cytokine pre-exposure were scraped and resuspended in 25 ml of assay buffer (100 NaCl, 20 mM HEPES, pH 7.0) supplemented with a cOmplete mini EDTA-free protease mixture tablet (Sigma). Cells in suspension were fragmented by 20 passages through a high-shear fluid processor at 120 p.s.i. (Microfluidics). The resultant membrane vesicles were collected by ultracentrifugation at 258,000 × *g* for 60 min. mAb20 immunoblotting analysis indicated that all cellular ZnT8 was recovered in the pellet. The membrane pellet was then homogenized in 0.5 ml of assay buffer and sonicated in an ice-chilled cup-horn sonicator until vesicle turbidity disappeared completely, indicating the formation of small unilamellar vesicles (SUVs) with diameters around 100 nm (82). Quantification of total protein amounts in SUVs indicated no significant difference with and without cytokine exposure.

### *Co-immunoprecipitation*

The binding capacity of mAb20-PEG5K-Dynabeads or anti-BAP31-PEG5K-Dynabeads was first determined by dose titrations of SUVs to estimate the saturating SUV concentration for a given amount of antibody-conjugated beads based on mAb20 or anti-BAP31 immunoblotting analysis of SUVs eluted from the beads. A 1.2-fold excess of beads was used for all experiments to ensure a ~50% depletion of ZnT8-containing SUVs and a >95% depletion of BAP31-containing SUVs by respective affinity beads. The co-immunoprecipitation experiments were performed by incubating an aliquot of SUVs and antibody-conjugated beads at room temperature for 2 h with 0.5% BSA as a blocking reagent. The unbound SUVs remained in the flow-through while bound SUVs were washed three times with assay buffer plus 0.1% BSA and then SDS-eluted by 1× Laemmli sample buffer. The amounts of ZnT8 in total SUVs, flow-through, and bead elution were analyzed by mAb20 immunoblotting and quantified by ImageJ as described above.

### *GSIS and insulin quantification*

EndoC-$\beta$H1 cells with dose titrations of Glc + PA, zinc, or a cytokine mixture in a 96-well plate were switched to a Krebs buffer (Alfa Aesar, catalog no. J67795). After cell starvation in Krebs buffer for 1 h, EndoC-$\beta$H1 cells were replaced with fresh Krebs buffer containing 20 mM glucose plus 45 $\mu$M isobutylmethylxanthine. After 45 min, the Krebs buffer was collected for measurement of secreted insulin. Cells were then lysed by 100 $\mu$l/well Krebs buffer with 1% dodecyl maltoside. Total insulin content was measured in 100-fold diluted cell lysate. A homogeneous time-resolved fluorescence– based ultrasensitive insulin kit (Cisbio, catalog no. 62IN2PEG) was used to detect both secreted and total insulin as described previously (60).

### *Transcriptome profiling*

RNA-Seq mRNA profiles of EndoC-$\beta$H1 cells with or without 1× cytokine exposure for 24 h were generated by deep sequencing using an Illumina HiSeq2500 system. Cells were collected, washed by PBS, and lysed for total RNA extraction using an RNeasy Mini Kit (Qiagen, catalog no. 74104). The NEBNext Poly(A) Magnetic Isolation Module (New England Biolabs, catalog no. E7490) and the NEBNext Ultra II Directional RNA Library Prep Kit for Illumina (catalog no. E7765) were used to generate libraries. The BioAnalyzer was used for quality control of the libraries to ensure adequate concentration and appropriate fragment size. The resulting library insert size was 200–500 bp with a median size around 300 bp. Libraries were uniquely barcoded and pooled for sequencing. Reads were demultiplexed using Illumina's bcl2fastq2. Read quality was checked for each sample using FastQC version 0.10.1, and then they were imported into STAR version 2.5.2b for alignment into BAM files. The aligned reads were assembled with CLASS version 2.1.7, for each sample to create transcript models (transfrags). The resulted gtf files were fed to Stringtie-merge (version 1.3.6) to create a nonredundant set of transcripts, which was used in a later analysis of differential expression. Cuffdiff version 2.2.1 was run on each sample to obtain FPKM values found in the FPKM_matrix.xlsx file. Both Cuffdiff and DESeq were used to look for significant changes in transcript expression. DESeq output was split into two files, containing the transfrags that were annotated (DESeq_results_gn.csv) and the ones that could not be assigned to a known gene (DESeq_results_no_gn.csv).Cuffdiff_*_exp.diff.txt files were generated with Cuffdiff. These tab delimited files contain the feature_id, gene name, locus, sample names, test_status, FPKM values for each gene or transcript in both samples, log -fold change FPKM*y*/FPKM*x*, value of test statistics used to compute

significance of the observed change in FPKM, *p* value, and *q* values. FPKM values and the standard deviations per sample were summarized in FPKM_matrix.xlsx.

### *SLC30A8 knockdown*

To perform gene silencing by RNAi, a master mix of Opti-MEM reduced serum-free medium (Gibco, catalog no. 31985-062) was premixed with 0.4% RNAiMAX transfection reagent (Invitrogen, catalog no. 13778-100) and 75 nM ZnT8-targeting or scrambled siRNA (OriGene catalog no. SR325944). The solution was then incubated at room temperature for 10 min to form siRNA-lipid complexes before 50 $\mu$l of the master mix was added to each well in a 96-well plate. Cells resuspended in standard culturing media were added in a 1:1 volume to give $7 \times 10^4$ cells/well. After 24 h, the transfection media were replaced with complete culturing media. After additional 2 days, cells were exposed to 1× cytokine mixture, followed by immunoblotting and cytotoxicity analysis as described above.

*Author contributions*—C. M. data curation; C. M. and D. F. methodology; C. M. writing-review and editing; D. F. conceptualization; D. F. resources; D. F. funding acquisition; D. F. writing-original draft.

*Acknowledgments—We thank Barbara Smith (microscopy facility of the Johns Hopkins University School of Medicine) for assistance in cell imaging and processing, David Mohr and Jinshui Fan (Genetic Resources Core Facility of the Johns Hopkins Institute of Genetic Medicine) for RNA-Seq library preparation and Illumina sequencing, and Liliana Florea and Corina Antonescu (Computational Biology Consulting Core of the Johns Hopkins School of Medicine) for RNA-Seq data analysis and GEO-NCBI submission. The Zeiss confocal microscope was funded through National Institutes of Health Shared Instrumentation Grant S10OD016374.*

## References

1. Schuit, F. C., In't Veld, P. A., and Pipeleers, D. G. (1988) Glucose stimulates proinsulin biosynthesis by a dose-dependent recruitment of pancreatic beta cells. *Proc. Natl. Acad. Sci. U.S.A.* **85,** 3865–3869 CrossRef Medline
2. Dodson, G., and Steiner, D. (1998) The role of assembly in insulin's biosynthesis. *Curr. Opin. Struct. Biol.* **8,** 189–194 CrossRef Medline
3. Foster, M. C., Leapman, R. D., Li, M. X., and Atwater, I. (1993) Elemental composition of secretory granules in pancreatic islets of Langerhans. *Biophys. J.* **64,** 525–532 CrossRef Medline
4. Vinkenborg, J. L., Nicolson, T. J., Bellomo, E. A., Koay, M. S., Rutter, G. A., and Merkx, M. (2009) Genetically encoded FRET sensors to monitor intracellular $Zn^{2+}$ homeostasis. *Nat. Methods* **6,** 737–740 CrossRef Medline
5. Huang, L. (2014) Zinc and its transporters, pancreatic beta-cells, and insulin metabolism. *Vitam. Horm.* **95,** 365–390 CrossRef Medline
6. Kambe, T., Hashimoto, A., and Fujimoto, S. (2014) Current understanding of ZIP and ZnT zinc transporters in human health and diseases. *Cell Mol. Life Sci.* **71,** 3281–3295 CrossRef Medline
7. Lemaire, K., Chimienti, F., and Schuit, F. (2012) Zinc transporters and their role in the pancreatic beta-cell. *J. Diabetes Investig.* **3,** 202–211 CrossRef Medline
8. Segerstolpe, Å., Palasantza, A., Eliasson, P., Andersson, E. M., Andréasson, A. C., Sun, X., Picelli, S., Sabirsh, A., Clausen, M., Bjursell, M. K., Smith, D. M., Kasper, M., Ämmälä, C., and Sandberg, R. (2016) Single-cell transcriptome profiling of human pancreatic islets in health and type 2 diabetes. *Cell Metab.* **24,** 593–607 CrossRef Medline
9. Wenzlau, J. M., Juhl, K., Yu, L., Moua, O., Sarkar, S. A., Gottlieb, P., Rewers, M., Eisenbarth, G. S., Jensen, J., Davidson, H. W., and Hutton, J. C. (2007) The cation efflux transporter ZnT8 (Slc30A8) is a major autoantigen in human type 1 diabetes. *Proc. Natl. Acad. Sci. U.S.A.* **104,** 17040–17045 CrossRef Medline
10. Énée, É., Kratzer, R., Arnoux, J. B., Barilleau, E., Hamel, Y., Marchi, C., Beltrand, J., Michaud, B., Chatenoud, L., Robert, J. J., and van Endert, P. (2012) ZnT8 is a major $CD8^+$ T cell-recognized autoantigen in pediatric type 1 diabetes. *Diabetes* **61,** 1779–1784 CrossRef Medline
11. Sladek, R., Rocheleau, G., Rung, J., Dina, C., Shen, L., Serre, D., Boutin, P., Vincent, D., Belisle, A., Hadjadj, S., Balkau, B., Heude, B., Charpentier, G., Hudson, T. J., Montpetit, A., *et al.* (2007) A genome-wide association study identifies novel risk loci for type 2 diabetes. *Nature* **445,** 881–885 CrossRef Medline
12. Flannick, J., Thorleifsson, G., Beer, N. L., Jacobs, S. B., Grarup, N., Burtt, N. P., Mahajan, A., Fuchsberger, C., Atzmon, G., Benediktsson, R., Blangero, J., Bowden, D. W., Brandslund, I., Brosnan, J., Burslem, F., *et al.* (2014) Loss-of-function mutations in SLC30A8 protect against type 2 diabetes. *Nat. Genet.* **46,** 357–363 CrossRef Medline
13. Nicolson, T. J., Bellomo, E. A., Wijesekara, N., Loder, M. K., Baldwin, J. M., Gyulkhandanyan, A. V., Koshkin, V., Tarasov, A. I., Carzaniga, R., Kronenberger, K., Taneja, T. K., da Silva Xavier, G., Libert, S., Froguel, P., Scharfmann, R., *et al.* (2009) Insulin storage and glucose homeostasis in mice null for the granule zinc transporter ZnT8 and studies of the type 2 diabetes-associated variants. *Diabetes* **58,** 2070–2083 CrossRef Medline
14. Wijesekara, N., Dai, F. F., Hardy, A. B., Giglou, P. R., Bhattacharjee, A., Koshkin, V., Chimienti, F., Gaisano, H. Y., Rutter, G. A., and Wheeler, M. B. (2010) Beta cell-specific Znt8 deletion in mice causes marked defects in insulin processing, crystallisation and secretion. *Diabetologia* **53,** 1656–1668 CrossRef Medline
15. Pound, L. D., Sarkar, S. A., Benninger, R. K., Wang, Y., Suwanichkul, A., Shadoan, M. K., Printz, R. L., Oeser, J. K., Lee, C. E., Piston, D. W., McGuinness, O. P., Hutton, J. C., Powell, D. R., and O'Brien, R. M. (2009) Deletion of the mouse Slc30a8 gene encoding zinc transporter-8 results in impaired insulin secretion. *Biochem. J.* **421,** 371–376 CrossRef Medline
16. Lemaire, K., Ravier, M. A., Schraenen, A., Creemers, J. W., Van de Plas, R., Granvik, M., Van Lommel, L., Waelkens, E., Chimienti, F., Rutter, G. A., Gilon, P., in't Veld, P. A., and Schuit, F. C. (2009) Insulin crystallization depends on zinc transporter ZnT8 expression, but is not required for normal glucose homeostasis in mice. *Proc. Natl. Acad. Sci. U.S.A.* **106,** 14872–14877 CrossRef Medline
17. Pound, L. D., Sarkar, S. A., Ustione, A., Dadi, P. K., Shadoan, M. K., Lee, C. E., Walters, J. A., Shiota, M., McGuinness, O. P., Jacobson, D. A., Piston, D. W., Hutton, J. C., Powell, D. R., and O'Brien, R. M. (2012) The physiological effects of deleting the mouse SLC30A8 gene encoding zinc transporter-8 are influenced by gender and genetic background. *PLoS One* **7,** e40972 CrossRef Medline
18. Chabosseau, P., and Rutter, G. A. (2016) Zinc and diabetes. *Arch. Biochem. Biophys.* **611,** 79–85 CrossRef Medline
19. Saltiel, A. R., and Olefsky, J. M. (2017) Inflammatory mechanisms linking obesity and metabolic disease. *J. Clin. Invest.* **127,** 1–4 CrossRef Medline
20. Leahy, J. L., Cooper, H. E., Deal, D. A., and Weir, G. C. (1986) Chronic hyperglycemia is associated with impaired glucose influence on insulin secretion: a study in normal rats using chronic *in vivo* glucose infusions. *J. Clin. Invest.* **77,** 908–915 CrossRef Medline
21. Maedler, K., Spinas, G. A., Dyntar, D., Moritz, W., Kaiser, N., and Donath, M. Y. (2001) Distinct effects of saturated and monounsaturated fatty acids on beta-cell turnover and function. *Diabetes* **50,** 69–76 CrossRef Medline
22. Poitout, V., and Robertson, R. P. (2008) Glucolipotoxicity: fuel excess and beta-cell dysfunction. *Endocr. Rev.* **29,** 351–366 CrossRef Medline
23. Butcher, M. J., Hallinger, D., Garcia, E., Machida, Y., Chakrabarti, S., Nadler, J., Galkina, E. V., and Imai, Y. (2014) Association of proinflammatory cytokines and islet resident leucocytes with islet dysfunction in type 2 diabetes. *Diabetologia* **57,** 491–501 CrossRef Medline
24. Hotamisligil, G. S. (2017) Inflammation, metaflammation and immunometabolic disorders. *Nature* **542,** 177–185 CrossRef Medline
25. Donath, M. Y., and Shoelson, S. E. (2011) Type 2 diabetes as an inflammatory disease. *Nat. Rev. Immunol.* **11,** 98–107 CrossRef Medline
26. Tsai, S., Clemente-Casares, X., Revelo, X. S., Winer, S., and Winer, D. A. (2015) Are obesity-related insulin resistance and type 2 diabetes autoimmune diseases? *Diabetes* **64,** 1886–1897 CrossRef Medline

27. Zumsteg, U., Frigerio, S., and Holländer, G. A. (2000) Nitric oxide production and Fas surface expression mediate two independent pathways of cytokine-induced murine beta-cell damage. *Diabetes* **49,** 39–47 CrossRef Medline
28. Robertson, R. P., Harmon, J., Tran, P. O., and Poitout, V. (2004) Beta-cell glucose toxicity, lipotoxicity, and chronic oxidative stress in type 2 diabetes. *Diabetes* **53,** Suppl. 1, S119–S124 CrossRef Medline
29. Eide, D. J. (2011) The oxidative stress of zinc deficiency. *Metallomics* **3,** 1124–1129 CrossRef Medline
30. Homma, K., Fujisawa, T., Tsuburaya, N., Yamaguchi, N., Kadowaki, H., Takeda, K., Nishitoh, H., Matsuzawa, A., Naguro, I., and Ichijo, H. (2013) SOD1 as a molecular switch for initiating the homeostatic ER stress response under zinc deficiency. *Mol. Cell* **52,** 75–86 CrossRef Medline
31. Fonseca, S. G., Burcin, M., Gromada, J., and Urano, F. (2009) Endoplasmic reticulum stress in beta-cells and development of diabetes. *Curr. Opin. Pharmacol.* **9,** 763–770 CrossRef Medline
32. Merriman, C., Li, H., Li, H., and Fu, D. (2018) Highly specific monoclonal antibodies for allosteric inhibition and immunodetection of the human pancreatic zinc transporter ZnT8. *J. Biol. Chem.* **293,** 16206–16216 CrossRef Medline
33. Merriman, C., Huang, Q., Gu, W., Yu, L., and Fu, D. (2018) A subclass of serum anti-ZnT8 antibodies directed to the surface of live pancreatic beta-cells. *J. Biol. Chem.* **293,** 579–587 CrossRef Medline
34. Merriman, C., Huang, Q., Rutter, G. A., and Fu, D. (2016) Lipid-tuned zinc transport activity of human ZnT8 protein correlates with risk for type-2 diabetes. *J. Biol. Chem.* **291,** 26950–26957 CrossRef Medline
35. Poitout, V., Amyot, J., Semache, M., Zarrouki, B., Hagman, D., and Fontés, G. (2010) Glucolipotoxicity of the pancreatic beta cell. *Biochim. Biophys. Acta* **1801,** 289–298 CrossRef Medline
36. Eizirik, D. L., Colli, M. L., and Ortis, F. (2009) The role of inflammation in insulitis and beta-cell loss in type 1 diabetes. *Nat. Rev. Endocrinol.* **5,** 219–226 CrossRef Medline
37. Hakonen, E., Chandra, V., Fogarty, C. L., Yu, N. Y., Ustinov, J., Katayama, S., Galli, E., Danilova, T., Lindholm, P., Vartiainen, A., Einarsdottir, E., Krjutškov, K., Kere, J., Saarma, M., Lindahl, M., and Otonkoski, T. (2018) MANF protects human pancreatic beta cells against stress-induced cell death. *Diabetologia* **61,** 2202–2214 CrossRef Medline
38. Gurgul-Convey, E., Mehmeti, I., Plötz, T., Jörns, A., and Lenzen, S. (2016) Sensitivity profile of the human EndoC-betaH1 beta cell line to proinflammatory cytokines. *Diabetologia* **59,** 2125–2133 CrossRef Medline
39. Thul, P. J., Åkesson, L., Wiking, M., Mahdessian, D., Geladaki, A., Ait Blal, H., Alm, T., Asplund, A., Björk, L., Breckels, L. M., Bäckström, A., Danielsson, F., Fagerberg, L., Fall, J., Gatto, L., *et al.* (2017) A subcellular map of the human proteome. *Science* **356,** eaal3321 CrossRef Medline
40. Davidson, H. W., Wenzlau, J. M., and O'Brien, R. M. (2014) Zinc transporter 8 (ZnT8) and beta cell function. *Trends Endocrinol. Metab.* **25,** 415–424 CrossRef Medline
41. Chimienti, F., Devergnas, S., Favier, A., and Seve, M. (2004) Identification and cloning of a beta-cell-specific zinc transporter, ZnT-8, localized into insulin secretory granules. *Diabetes* **53,** 2330–2337 CrossRef Medline
42. Solimena, M., Dirkx, R., Jr, Hermel, J. M., Pleasic-Williams, S., Shapiro, J. A., Caron, L., and Rabin, D. U. (1996) ICA 512, an autoantigen of type I diabetes, is an intrinsic membrane protein of neurosecretory granules. *EMBO J.* **15,** 2102–2114 CrossRef Medline
43. Regazzi, R., Wollheim, C. B., Lang, J., Theler, J. M., Rossetto, O., Montecucco, C., Sadoul, K., Weller, U., Palmer, M., and Thorens, B. (1995) VAMP-2 and cellubrevin are expressed in pancreatic beta-cells and are essential for $Ca^{2+}$- but not for GTPγS-induced insulin secretion. *EMBO J.* **14,** 2723–2730 CrossRef Medline
44. Kay, T. W., Campbell, I. L., Oxbrow, L., and Harrison, L. C. (1991) Overexpression of class I major histocompatibility complex accompanies insulitis in the non-obese diabetic mouse and is prevented by anti-interferon-γ antibody. *Diabetologia* **34,** 779–785 CrossRef Medline
45. Scheuner, D., and Kaufman, R. J. (2008) The unfolded protein response: a pathway that links insulin demand with beta-cell failure and diabetes. *Endocr. Rev.* **29,** 317–333 CrossRef Medline
46. Farino, Z. J., Morgenstern, T. J., Vallaghe, J., Gregor, N., Donthamsetti, P., Harris, P. E., Pierre, N., Freyberg, R., Charrier-Savournin, F., Javitch, J. A., and Freyberg, Z. (2016) Development of a rapid insulin assay by homogenous time-resolved fluorescence. *PLoS One* **11,** e0148684 CrossRef Medline
47. Kharroubi, I., Ladrière, L., Cardozo, A. K., Dogusan, Z., Cnop, M., and Eizirik, D. L. (2004) Free fatty acids and cytokines induce pancreatic beta-cell apoptosis by different mechanisms: role of nuclear factor-κB and endoplasmic reticulum stress. *Endocrinology* **145,** 5087–5096 CrossRef Medline
48. Akerfeldt, M. C., Howes, J., Chan, J. Y., Stevens, V. A., Boubenna, N., McGuire, H. M., King, C., Biden, T. J., and Laybutt, D. R. (2008) Cytokine-induced beta-cell death is independent of endoplasmic reticulum stress signaling. *Diabetes* **57,** 3034–3044 CrossRef Medline
49. Cnop, M., Welsh, N., Jonas, J. C., Jörns, A., Lenzen, S., and Eizirik, D. L. (2005) Mechanisms of pancreatic beta-cell death in type 1 and type 2 diabetes: many differences, few similarities. *Diabetes* **54,** Suppl. 2, S97–S107 CrossRef Medline
50. Li, Z., Liu, H., Niu, Z., Zhong, W., Xue, M., Wang, J., Yang, F., Zhou, Y., Zhou, Y., Xu, T., and Hou, J. (2018) Temporal proteomic analysis of pancreatic beta-cells in response to lipotoxicity and glucolipotoxicity. *Mol. Cell Proteomics* **17,** 2119–2131 CrossRef Medline
51. Busch, A. K., Gurisik, E., Cordery, D. V., Sudlow, M., Denyer, G. S., Laybutt, D. R., Hughes, W. E., and Biden, T. J. (2005) Increased fatty acid desaturation and enhanced expression of stearoyl coenzyme A desaturase protects pancreatic beta-cells from lipoapoptosis. *Diabetes* **54,** 2917–2924 CrossRef Medline
52. Rojas, J., Bermudez, V., Palmar, J., Martínez, M. S., Olivar, L. C., Nava, M., Tomey, D., Rojas, M., Salazar, J., Garicano, C., and Velasco, M. (2018) Pancreatic beta cell death: novel potential mechanisms in diabetes therapy. *J. Diabetes Res.* **2018,** 9601801 CrossRef Medline
53. Fabregat, A., Jupe, S., Matthews, L., Sidiropoulos, K., Gillespie, M., Garapati, P., Haw, R., Jassal, B., Korninger, F., May, B., Milacic, M., Roca, C. D., Rothfels, K., Sevilla, C., Shamovsky, V., *et al.* (2018) The reactome pathway knowledgebase. *Nucleic Acids Res.* **46,** D649–D655 CrossRef Medline
54. Murata, S., Takahama, Y., Kasahara, M., and Tanaka, K. (2018) The immunoproteasome and thymoproteasome: functions, evolution and human disease. *Nat. Immunol.* **19,** 923–931 CrossRef Medline
55. Arvan, P., Pietropaolo, M., Ostrov, D., and Rhodes, C. J. (2012) Islet autoantigens: structure, function, localization, and regulation. *Cold Spring Harb. Perspect. Med.* **2,** a007658 CrossRef Medline
56. Dudek, N. L., Tan, C. T., Gorasia, D. G., Croft, N. P., Illing, P. T., and Purcell, A. W. (2012) Constitutive and inflammatory immunopeptidome of pancreatic beta-cells. *Diabetes* **61,** 3018–3025 CrossRef Medline
57. Jarchum, I., Baker, J. C., Yamada, T., Takaki, T., Marron, M. P., Serreze, D. V., and DiLorenzo, T. P. (2007) *In vivo* cytotoxicity of insulin-specific $CD8^+$ T-cells in HLA-A*0201 transgenic NOD mice. *Diabetes* **56,** 2551–2560 CrossRef Medline
58. Scotto, M., Afonso, G., Larger, E., Raverdy, C., Lemonnier, F. A., Carel, J. C., Dubois-Laforgue, D., Baz, B., Levy, D., Gautier, J. F., Launay, O., Bruno, G., Boitard, C., Sechi, L. A., Hutton, J. C., *et al.* (2012) Zinc transporter (ZnT)8(186–194) is an immunodominant $CD8^+$ T cell epitope in HLA-$A2^+$ type 1 diabetic patients. *Diabetologia* **55,** 2026–2031 CrossRef Medline
59. Meng, L., Mohan, R., Kwok, B. H., Elofsson, M., Sin, N., and Crews, C. M. (1999) Epoxomicin, a potent and selective proteasome inhibitor, exhibits *in vivo* antiinflammatory activity. *Proc. Natl. Acad. Sci. U.S.A.* **96,** 10403–10408 CrossRef Medline
60. Huang, Q., Merriman, C., Zhang, H., and Fu, D. (2017) Coupling of insulin secretion and display of a granule-resident zinc transporter ZnT8 on the surface of pancreatic beta cells. *J. Biol. Chem.* **292,** 4034–4043 CrossRef Medline
61. Wan, H., Merriman, C., Atkinson, M. A., Wasserfall, C. H., Mcgrail, K. M., Liang, Y., Fu, D., and Dai, H. (2017) Proteoliposome-based full-length ZnT8 self-antigen for type 1 diabetes diagnosis on a plasmonic platform. *Proc. Natl. Acad. Sci. U.S.A.* **114,** 10196–10201 CrossRef Medline
62. El Muayed, M., Billings, L. K., Raja, M. R., Zhang, X., Park, P. J., Newman, M. V., Kaufman, D. B., O'Halloran, T. V., and Lowe, W. L., Jr. (2010) Acute cytokine-mediated downregulation of the zinc transporter ZnT8 alters

pancreatic beta-cell function. *J. Endocrinol.* **206,** 159–169 CrossRef Medline

63. Egefjord, L., Jensen, J. L., Bang-Berthelsen, C. H., Petersen, A. B., Smidt, K., Schmitz, O., Karlsen, A. E., Pociot, F., Chimienti, F., Rungby, J., and Magnusson, N. E. (2009) Zinc transporter gene expression is regulated by pro-inflammatory cytokines: a potential role for zinc transporters in beta-cell apoptosis? *BMC Endocr. Disord.* **9,** 7 CrossRef Medline
64. Cheng, L., Zhang, D., and Chen, B. (2016) Tumor necrosis factor α-induced protein-3 protects zinc transporter 8 against proinflammatory cytokine-induced downregulation. *Exp. Ther. Med.* **12,** 1509–1514 CrossRef Medline
65. Wong, W. P., Allen, N. B., Meyers, M. S., Link, E. O., Zhang, X., MacRenaris, K. W., and El Muayed, M. (2017) Exploring the association between demographics, SLC30A8 genotype, and human islet content of zinc, cadmium, copper, iron, manganese and nickel. *Sci. Rep.* **7,** 473 CrossRef Medline
66. Parsons, D. S., Hogstrand, C., and Maret, W. (2018) The C-terminal cytosolic domain of the human zinc transporter ZnT8 and its diabetes risk variant. *FEBS J.* **285,** 1237–1250 CrossRef Medline
67. Flannick, J., Mercader, J. M., Fuchsberger, C., Udler, M. S., Mahajan, A., Wessel, J., Teslovich, T. M., Caulkins, L., Koesterer, R., Barajas-Olmos, F., Blackwell, T. W., Boerwinkle, E., Brody, J. A., Centeno-Cruz, F., Chen, L., *et al.* (2019) Exome sequencing of 20,791 cases of type 2 diabetes and 24,440 controls. *Nature* **570,** 71–76 CrossRef Medline
68. Chabosseau, P., Tuncay, E., Meur, G., Bellomo, E. A., Hessels, A., Hughes, S., Johnson, P. R., Bugliani, M., Marchetti, P., Turan, B., Lyon, A. R., Merkx, M., and Rutter, G. A. (2014) Mitochondrial and ER-targeted eCALWY probes reveal high levels of free $Zn^{2+}$. *ACS Chem. Biol.* **9,** 2111–2120 CrossRef Medline
69. Liu, Y., Batchuluun, B., Ho, L., Zhu, D., Prentice, K. J., Bhattacharjee, A., Zhang, M., Pourasgari, F., Hardy, A. B., Taylor, K. M., Gaisano, H., Dai, F. F., and Wheeler, M. B. (2015) Characterization of zinc influx transporters (ZIPs) in pancreatic beta cells: roles in regulating cytosolic zinc homeostasis and insulin secretion. *J. Biol. Chem.* **290,** 18757–18769 CrossRef Medline
70. Taylor, K. M., Hiscox, S., Nicholson, R. I., Hogstrand, C., and Kille, P. (2012) Protein kinase CK2 triggers cytosolic zinc signaling pathways by phosphorylation of zinc channel ZIP7. *Sci. Signal.* **5,** ra11 CrossRef Medline
71. Woodruff, G., Bouwkamp, C. G., de Vrij, F. M., Lovenberg, T., Bonaventure, P., Kushner, S. A., and Harrington, A. W. (2018) The zinc transporter SLC39A7 (ZIP7) is essential for regulation of cytosolic zinc levels. *Mol. Pharmacol.* **94,** 1092–1100 CrossRef Medline
72. Ohashi, W., Kimura, S., Iwanaga, T., Furusawa, Y., Irié, T., Izumi, H., Watanabe, T., Hijikata, A., Hara, T., Ohara, O., Koseki, H., Sato, T., Robine, S., Mori, H., Hattori, Y., *et al.* (2016) Zinc transporter SLC39A7/ZIP7 promotes intestinal epithelial self-renewal by resolving ER stress. *PLoS Genet.* **12,** e1006349 CrossRef Medline
73. Tuncay, E., Bitirim, V. C., Durak, A., Carrat, G. R. J., Taylor, K. M., Rutter, G. A., and Turan, B. (2017) Hyperglycemia-induced changes in ZIP7 and ZnT7 expression cause $Zn^{2+}$ release from the sarco(endo)plasmic reticulum and mediate ER stress in the heart. *Diabetes* **66,** 1346–1358 CrossRef Medline
74. Liu, M., Hodish, I., Rhodes, C. J., and Arvan, P. (2007) Proinsulin maturation, misfolding, and proteotoxicity. *Proc. Natl. Acad. Sci. U.S.A.* **104,** 15841–15846 CrossRef Medline
75. Wenzlau, J. M., and Hutton, J. C. (2013) Novel diabetes autoantibodies and prediction of type 1 diabetes. *Curr. Diab. Rep.* **13,** 608–615 CrossRef Medline
76. Li, S., Li, H., Chen, B., Lu, D., Deng, W., Jiang, Y., Zhou, Z., and Yang, Z. (2013) Identification of novel HLA-A 0201-restricted cytotoxic T lymphocyte epitopes from zinc transporter 8. *Vaccine* **31,** 1610–1615 CrossRef Medline
77. Yu, C., Burns, J. C., Robinson, W. H., Utz, P. J., Ho, P. P., Steinman, L., and Frey, A. B. (2016) Identification of candidate tolerogenic $CD8^+$ T cell epitopes for therapy of type 1 diabetes in the NOD mouse model. *J. Diabetes Res.* **2016,** 9083103 CrossRef Medline
78. Liston, A., Todd, J. A., and Lagou, V. (2017) Beta-cell fragility as a common underlying risk factor in type 1 and type 2 diabetes. *Trends Mol. Med.* **23,** 181–194 CrossRef Medline
79. Ravassard, P., Hazhouz, Y., Pechberty, S., Bricout-Neveu, E., Armanet, M., Czernichow, P., and Scharfmann, R. (2011) A genetically engineered human pancreatic beta cell line exhibiting glucose-inducible insulin secretion. *J. Clin. Invest.* **121,** 3589–3597 CrossRef Medline
80. Barlow, J., and Affourtit, C. (2013) Novel insights into pancreatic beta-cell glucolipotoxicity from real-time functional analysis of mitochondrial energy metabolism in INS-1E insulinoma cells. *Biochem. J.* **456,** 417–426 CrossRef Medline
81. Li, Q., Lau, A., Morris, T. J., Guo, L., Fordyce, C. B., and Stanley, E. F. (2004) A syntaxin 1, $G\alpha_o$, and N-type calcium channel complex at a presynaptic nerve terminal: analysis by quantitative immunocolocalization. *J. Neurosci.* **24,** 4070–4081 CrossRef Medline
82. Szoka, F., Jr., and Papahadjopoulos, D. (1980) Comparative properties and methods of preparation of lipid vesicles (liposomes). *Annu. Rev. Biophys. Bioeng.* **9,** 467–508 CrossRef Medline
83. Fred, R. G., Kappe, C., Ameur, A., Cen, J., Bergsten, P., Ravassard, P., Scharfmann, R., and Welsh, N. (2015) Role of the AMP kinase in cytokine-induced human EndoC-betaH1 cell death. *Mol. Cell Endocrinol.* **414,** 53–63 CrossRef Medline